Part II

Superconducting bars and arrays in the critical state

CHAPTER 6

The magnetic energy minimization procedure

In the first part of this thesis, our study has been focused on linear homogenous isotropical (LHI) materials. In the remainder we shall deal with hard superconductors, which are highly nonlinear hysteretic materials. For such materials we can no longer use the numerical method presented in chapter 3. Moreover, hard superconductors are very interesting for applications (§2.3.3). Actually, all superconducting materials with applications, including high-temperature superconductors are hard.

In this chapter we present a numerical model, based on the critical-state model (Sec. 2.3.3), which is suitable for hard superconductors. This model is developed for an infinitely long superconductor along the z axis with z-independent cross-section and finite transverse dimensions. We will study the cases of a transverse applied field $H_{\rm a}$ in the y direction or a transport current I in the z direction, so that the current density is parallel to the z axis. Although for the transport case this model is useful for any cross-section shape, for the magnetic case the system must have mirror symmetry with respect to the yz plane[1], so that $J_z(x,y) = -J_z(-x,y)$. This is so because to apply the model it is necessary to know *a priory* the geometry of all the closed current lines.

Almost all the critical-state model calculations presented in this thesis are carried out using the magnetic energy minimization (MEM) procedure [72], based on the critical-state model. Although the model allows a magnetic induction dependence of J_c, for the present thesis we only study the case of a constant critical current density J_c. In this chapter we extent the MEM procedure that was, developed for cylinders in applied magnetic fields (dc or ac and uniform or nonuniform) [72, 73, 74, 6] to the infinitely long geometry, both for transverse applied fields and the transport case.

By the MEM procedure one finds the new induced current distribution which minimizes the magnetic energy after an external parameter variation, either the applied field

[1] Actually it is enough that the system has inversion point symmetry, so that $J_z(x,y) = -J_z(-x,-y)$.

H_a or the transport current I. Although a similar principle is used in other models [75, 76, 77, 78, 79, 80], we use a minimization technique that has been not only developed independently, but also it is optimum, considering computing time and accuracy, for the calculation of the electromagnetic properties under an ac applied field or current.

6.1 Case of uniform applied field

In this section we develop the MEM procedure for the case of a transverse uniform applied field. Although this model is suitable for any cross-section with mirror symmetry with respect to the yz plane, we concentrate on the study of arrangements of n_f superconducting filaments with rectangular cross-section (strips) of dimensions $2a \times 2b$ in the x and y directions, respectively (Fig. 6.1).

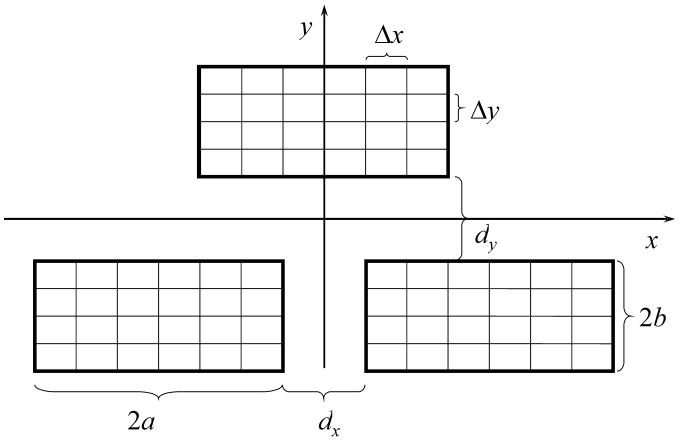

Figure 6.1: Sketch for an example of cross-section made of rectangular strips which can be calculated using our numerical method. A division into elements of the cross-section is shown.

6.1.1 Magnetic energy

The MEM procedure involves magnetic energy W per unit length, that is for an infinitely long circuit [12]

$$W = \frac{1}{2}\int_{S_{xy}} J_z A_{z,J} \mathrm{d}S + \int_{S_{xy}} J_z A_{z,e} \mathrm{d}S, \tag{6.1}$$

where S_{xy} is the whole xy planar surface, $A_{z,J}$ is the vector potential created by the current distribution and $A_{z,e}$ is the vector potential corresponding to an external applied field, if present. We will consider the gauge $\nabla \cdot \mathbf{A} = 0$, so that $A_{z,e} = -\mu_0 x H_a$ for a uniform H_a, and

$$A_{z,J}(\mathbf{r}) = -\frac{\mu_0}{4\pi}\int_{S_{xy}} J_z(\mathbf{r}') \ln\left[(x-x')^2 + (y-y')^2\right] \mathrm{d}S'. \tag{6.2}$$

The energy and flux minimization in the critical state was previously discussed by Prigozhin [75, 76], Badia *et al* [77, 78, 81], Chaddah and co-workers [82, 83] and Sanchez and Navau [72, 73]. We note that the functional of equation (14) in reference [76] which has to be minimized to find the current profile corresponds to the magnetic energy in equation (6.1) if the considered values of H_a and I are reached from the zero-field cooled state.

6.1.2 Current density calculation

We now describe how we calculate the current distribution by means of the MEM procedure. Once the current profiles are known, all the other relevant magnetic properties, such as the magnetic induction, magnetization, ac susceptibility or ac loss, can be easily deduced. To apply the MEM method it is necessary to divide the superconducting region into elements.

We start with the procedure for the initial magnetization curve, that is, if the applied field H_a is reached from the zero-field cooled state.

Discretization and formalism

Each superconducting filament is divided into $2n_x \times 2n_y$ elements with dimensions $a/n_x \times b/n_y$; critical current density is assumed to be uniform in each element. We will allow the current density to change in steps below J_c, that is, $J = mJ_c/m_m$ with m being an integer from 1 to m_m. As discussed in Ref. [84], the allowance of current densities lower than J_c reduces the discretization error in the ac loss calculation. Actually, there only appears $0 < |J| < J_c$ within one layer of one-element width beyond the $J = J_c$ front. This layer simulates much better the effect of a smoothly curved front.

Simply connected shapes

The main condition for applying the model is that one has to know in advance the direction of currents. In the case of multifilamentary cross-sections this issue has to be dealt with carefully; we will discuss about it in the next section.

We consider first the case of a simply connected superconductor with mirror symmetry with respect to the yz plane. For this case the current front is antisymmetric to this plane. Thus, we can consider that the pair of elements centered at (x, y) and $(-x, y)$ forms a circuit that is closed at infinity. The pair, or circuit, is labelled using the subscript j from 1 to $n = 2n_x n_y n_f$, being n_f the number of strips of the set and n the total number of elements in the $x > 0$ portion of the set of strips. The sign of the current in circuit j, I_j, is taken as positive when the current of the element at $x > 0$ of the pair follows the positive z direction, and negative otherwise.

The MEM procedure to find the current profile under an applied field was originally formulated in [72, 73, 6] for cylinders, and then extended to the infinitely long geometry in [71, 85]. The procedure is described in the following. First we divide the

superconducting region into closed circuits. Then, for a given current distribution and applied field we find the nonsaturated circuit j where increasing its current from I_j to $I_j + |\Delta I|$ reduces the most the magnetic energy, being $\Delta I = J_c ab/(n_x n_y m_m)$. We then repeat the procedure until adding more current in any nonsaturated circuit increases the energy instead of lowering it. Once the current profile for a certain applied field H_a is calculated, the determination of the current profile for a higher applied field $H_\mathrm{a} + \Delta H_\mathrm{a}$ requires much less numerical calculations than when we start from the zero-field cooled state for the same value of the applied field.

The increment of magnetic energy as a consequence of changing the current in the circuit j from I_j to $I_j + \Delta I$ can be calculated from Eq. (6.1) as

$$\Delta W = \sum_{k=1}^{n} M_{jk} I_k \Delta I + \frac{1}{2} M_{jj} (\Delta I)^2 + 2\mu_0 H_\mathrm{a} x_j \Delta I, \tag{6.3}$$

where the first term is the energy variation owing to the presence of the former current distribution in the whole superconducting region, the second one is the self-interaction energy, the third term is the energy due to the uniform applied magnetic field, and M_{jk} are the self ($j = k$) and mutual ($j \neq k$) inductances between circuits.

The above mentioned grouping in pairs that form closed circuits allows the calculation of mutual inductances by means of Eq. (6.1) using $M_{jk} \equiv W_{jk}/(I_j I_k)$ and $M_{jj} \equiv 2W_{jj}/I_j^2$ [12], where W_{jk} is the energy of circuit j due to the current flowing in circuit k and W_{jj} is the self-energy of circuit j. For the present infinitely long geometry we calculate the inductances considering that the current flows through the whole cross-section of the elements and not only in their center, as done in [72, 73, 6]. This allows the exact calculation of self inductances and increases the numerical calculation accuracy. Furthermore, the self-energy per unit length of a single element carrying a current I_j is infinite, even if we consider the finite cross-section of the element [12]. The analytical expressions for the inductances in our case are calculated in [71].

Multifilamentary cross-sections. Interconnected and isolated cases.

For multifilamentary cross-sections we can consider two possibilities: isolated or interconnected cases. For the former we assume that the superconducting parts, or filaments, are electrically isolated to each other, so that the total current flowing through them must be null for the magnetic case. The interconnected case assumes that the superconducting filaments are connected at infinity, so that we do not have this restriction to the current density.

We now discuss two features that are needed to apply the MEM procedure to any superconductor geometry; this will help us to determine which modifications, if necessary, have to be done to adapt the MEM procedure to multifilamentary cross-section tapes.

The first condition to apply the MEM procedure is that one needs to know the shape of the closed current loops of the magnetically induced current for any applied

field value H_a. For cylinders the closed current loops are simply circular [72, 73, 6], while for simply-connected infinitely-long tapes they are made up by an infinite straight current in the z direction centered at (x, y) and by another one centered at $(-x, y)$, which form a closed circuit at infinity.

Another feature that has to be taken into account is the sign of the induced current, once the shape of the closed current loops is known. For simply connected geometries such as rectangular strips [87, 88, 75, 85], cylinders [89, 75, 90, 72, 73], and elliptical tapes [75, 32, 33, 91], current in the initial magnetization curve has the same sign for all circuits. This issue is also fulfilled for geometries with no gaps in the horizontal direction, such as vertical stacks of strips [92]. However, for geometries with gaps in the horizontal direction like horizontal arrays and matrices, the current in the initial magnetization curve may not have the same sign for all circuits.

As explained in the following subsections, the applicability of the mentioned two features is different when considering interconnected or isolated filaments. So, we need to consider these cases separately.

Interconnected filaments

For this case we can take the same closed current circuits as for simply connected cross-sections, which are the pairs of current elements centered at (x, y) and $(-x, y)$. We can take them in this way thanks to the mirror yz symmetry of the whole system and the fact that the filaments are interconnected at infinity, so that currents belonging to different filaments can be closed.

To determine if all circuits have the same sign, we perform preliminary numerical calculations letting the procedure choose which sign in each circuit is optimum to minimize the energy. After doing so, we see that in the initial magnetization curve and for a given H_a, the current sign is the same and positive for all circuits, except for very few circuits on the final current profile due to discretization error. Then, the currents of the filaments at the $x > 0$ region return to those in the $x < 0$ region, so that currents return through different filaments for all circuits except for those centered at $x = 0$. This result is expected, since this situation is what minimizes the most the magnetic energy, so it should be the one chosen when there are no restrictions.

Thus, we conclude that the numerical method and formulae for multifilamentary cross-sections with interconnected filaments is the same as for simply connected geometries.

Isolated filaments

The model used to describe mutually isolated filaments must take into account that all real current loops have to be closed inside each strip, so that there has to be the same amount of current following the negative z direction than the positive one inside each strip. In addition, although the current distribution in the whole tape has yz mirror symmetry with respect to the plane at $x = 0$, the current distribution in the individual strips is not necessarily symmetrical to their own vertical central plane.

Then, the features of the MEM procedure described above do not apply, so that we need to do significant modifications to the original numerical procedure.

The actual current loops in this case have the shape of two straight lines within the same strip carrying opposite currents and closed at infinity (solid lines in Fig. 6.2). These straight lines can be identified by the elements which the strips are divided in. The main difficulty is to know which pair of elements describes a closed current loop.

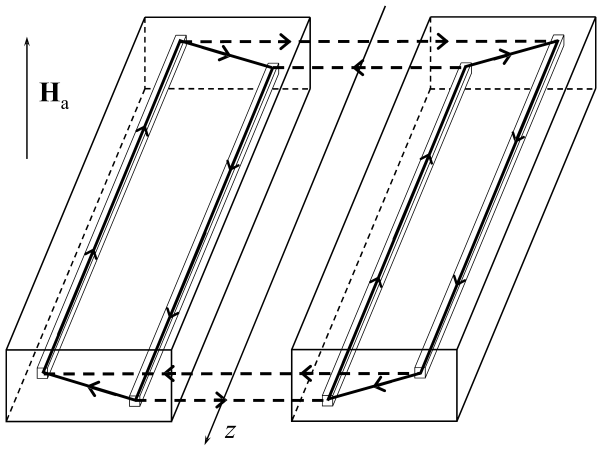

Figure 6.2: Sketch of the real closed current loops (solid thick lines) and those used in the simulation (dashed thick lines). The case of a horizontal array with two strips is drawn for simplicity. Four current elements are represented as elongated thin rectangular prisms where a single straight current flows following the z axis.

To help solving this problem we notice that, thanks to the overall mirror symmetry to the yz plane at $x = 0$, for any closed current loop in a filament at the $x > 0$ zone, there is another current loop set symmetrically in the corresponding filament in the $x < 0$ zone (Fig. 6.2). Furthermore, if we take as closed current loops the pairs of elements set symmetrically to the yz plane (dashed lines in Fig. 6.2), the total current distribution is the same except at the ends, which if we consider long enough strips does not modify the magnetic properties, including magnetic moment and energy. Consequently, since these symmetrical pairs of elements correspond to the closed loops used for simply connected cross-sections, the ΔW formula presented for that case (Sec. 6.3) is still applicable.

Taking these symmetrical pairs of elements as closed loops for the numerical procedure, as done above for interconnected strips, and the fact that actual current loops must close inside each strip, the MEM procedure for isolated strips becomes in this case:

1. For a given applied field H_a, a given current distribution, and for each pair of filaments set symmetrically to the yz plane (symmetrical pair of filaments) it is found i) the loop where setting a negative current would reduce the most the magnetic energy and ii) the loop where setting a positive current would rise it the least. These loops are referred to as a pair of loops.

2. The pair of loops that lowers the most the magnetic energy is selected among all those belonging to each symmetrical pair of filaments.

3. A current of the corresponding sign is set in the selected loops.

4. This procedure is repeated until setting current in the most energy-reducing pair of loops would not decrease the magnetic energy.

Notice that each pair of loops where current is set in the simulations stands for two real closed current loops belonging to each strip that constitute the symmetrical pair of strips (Fig. 6.2).

6.1.3 Magnetization, magnetic induction and ac susceptibility

In the initial magnetization curve, after using the energy minimization procedure to find the current profile, we can calculate the magnetization, the magnetic induction, and the magnetic field lines directly from the current distribution.

The magnetization, defined as the magnetic moment per unit volume (§2.1.1), has only one non-zero component, M_z, which can be calculated as

$$M_z = \frac{m_z}{4abn_f} = \frac{1}{4abn_f} \sum_{j=1}^{n} I_j \left(2x_j\right), \tag{6.4}$$

where m_z is the total magnetic moment of the superconducting tape. If we increase the applied field in steps of ΔH_a from the zero-field cooled state, we obtain the current profiles and the magnetization for a discrete set of H_a values between 0 and a maximum value H_m, so that the initial magnetization curve $M_i(H_\mathrm{a})$ can be obtained. Since we assume constant J_c, the reverse magnetization curve from H_m to $-H_m$ can be found using that [87, 89]

$$M_\mathrm{rev}(H_\mathrm{a}) = M_i(H_m) - 2M_i((H_m - H_\mathrm{a})/2), \tag{6.5}$$

and the returning curve, that closes the hysteresis loop, using

$$M_\mathrm{ret}(H_\mathrm{a}) = -M_\mathrm{rev}(-H_\mathrm{a}). \tag{6.6}$$

The two nonzero components of the magnetic flux density B_y and B_x are calculated as the addition of all the closed circuit contributions, which can be analytically obtained by integrating the Biot-Savart law [12].

The magnetic flux lines are calculated as in [88] using that for translational symmetry and for the gauge $\nabla \cdot \mathbf{A} = 0$, the level curves of the z component of the vector potential can be taken as the magnetic flux lines. The z component of the vector potential results from the contribution of all the elements pairs, whose analytical expressions are calculated and presented in Ref. [71][2].

[2]Formula (B4) in [71] has a typographical error. The two terms with arctangent should be $t^2 \arctan(d/t) + d^2 \arctan(t/d)$.

If we consider the application of an external ac field $H_a = H_m \cos\theta$, with $\theta = \omega t$, we can calculate the complex ac susceptibility $\chi_{ac} = \chi' - j\chi''$ by Fourier analysis using [93, 29]

$$\chi' = \frac{2}{\pi H_m} \int_0^\pi M_{rev}[H_a(\theta)] \cos\theta \mathrm{d}\theta, \tag{6.7}$$

$$\chi'' = \frac{2}{\pi H_m} \int_0^\pi M_{rev}[H_a(\theta)] \sin\theta \mathrm{d}\theta. \tag{6.8}$$

The energy loss per unit length and ac cycle Q_m due to the ac applied field amplitude H_m is related to χ'' by the expression [29, 89]

$$Q_m = \mu_0 \pi H_m^2 \chi''. \tag{6.9}$$

6.2 Transport case

We next present the adaptation of the MEM procedure to the situation where the superconductor carries a transport current I.

6.2.1 Internal magnetic energy

In order to apply the MEM procedure to the transport case, we imagine, following Norris [86], a circuit consisting of the superconducting tape and an outer perfectly conducting tube concentric with the tape with sufficiently large radius R, so that the current is uniformly distributed around its periphery. In the gauge of vector potential defined by Eq. (6.2) the vector potential generated by the tube is constant for $|\mathbf{r}| < R$. In addition, from Eq. (6.2) it can be deduced that if R is much larger than the dimensions of the superconducting tape cross-section, the vector potential generated by the superconductor on the tube is uniform with a value $-\mu_0 I/(2\pi) \ln R$. Then, the magnetic energy W can be deduced from Eq. (6.1) as

$$W = \frac{1}{2} \int_S J_z(\mathbf{r}) A_z(\mathbf{r}) \mathrm{d}S + \frac{\mu_0}{4\pi} I^2 \ln R \tag{6.10}$$

where S is the superconductor cross-section and A_z is the vector potential created by the supercurrent. The second term of Eq. (6.10) is constant for a fixed current I, so the only term in the energy which has to be minimized to determine the current distribution is

$$W' \equiv \frac{1}{2} \int_S J_z(\mathbf{r}) A_z(\mathbf{r}) \mathrm{d}S, \tag{6.11}$$

which we name as internal energy[3].

The minimization of the magnetic energy of Eqs. (6.1) or (6.11) to find the current density is carried out numerically, as presented below.

[3] We can obtain the same result if we consider that the current returns through an identical superconductor separated a large distance R, instead of the perfectly conducting tube.

6.2.2 Current density calculation

When the superconductor carries a transport current, one can distinguish between the case that the superconducting filaments are in parallel, so that the current I is freely shared among all filaments, or they are connected in series, so that we force that each filament carries the same net current. Although the latter case has some interest, we focus on the former, since this is the case found in actual superconducting tapes with neither twisting nor resistive barriers. Moreover, the case of filaments connected in parallel is simpler since we do not have to consider any restriction for the current density.

Next, we describe the MEM procedure for the transport case with filaments in parallel if the current I is reached from the zero-field cooled state. To do so, we divide the multifilamentary superconductor cross-section into elements in the same way as for the magnetic case in Sec. 6.1.2. For an already present numerical profile with current I, we increase the current for $\Delta I = J_c ab/(n_x n_y m_m)$ in the nonsaturated element where doing so the internal energy increases the least; the total current is therefore increased to $I + \Delta I$. This procedure is repeated from the zero-field cooled state ($I = 0$) up to the critical current I_c ($I_c = 4J_c abn_f$), obtaining all the profiles at a discretized set of dc current values in the process.

The internal energy variation $\Delta W'$ as a consequence of changing the current in the element j from I_j to $I_j + \Delta I$ can be calculated from Eq. (6.11) as

$$\Delta W' = \sum_{k=1}^{n} C_{jk} I_k \Delta I + \frac{1}{2} C_{jj} (\Delta I)^2, \tag{6.12}$$

where the factors C_{jk} are defined as the vector potential per unit current created by element k averaged over the cross-section of element j. These factors can be calculated analytically and are presented in Ref. [94].

6.2.3 Ac loss

If the superconductor carries an ac transport current $I = I_m \cos(\omega t)$, there appears ac loss. For constant J_c, the transport ac loss per cycle per unit length Q_t can be directly calculated from the current profile at $I = I_m$ as [86]

$$Q_t = 4 \int_S J_z(\mathbf{r}) \Phi(\mathbf{r}) \mathrm{d}S, \tag{6.13}$$

where $\Phi(\mathbf{r})$ is the magnetic flux per unit length between the flux-free core and position $\mathbf{r}$. We note that the current density at $I = I_m$ is the same as if the current were set from the zero-field cooled state. Furthermore, using $\mathbf{B} = \nabla \times \mathbf{A}$ and the Stokes theorem, one obtains that $\Phi(\mathbf{r})$ equals the vector potential difference between the flux-free core and position $\mathbf{r}$. Considering this and taking into account that the vector potential generated by the tube at R is uniform for $|\mathbf{r}| < R$ we deduce from Eq. (6.13) that

$$Q_t = 4 \int_S J_z(\mathbf{r}) \left[A_{z,c} - A_z(\mathbf{r}) \right] \mathrm{d}S, \tag{6.14}$$

where $A_{z,c}$ is the vector potential in the flux-free core.

The evaluation of Q_t from the numerical current profile yields to

$$Q_t = 4\left[I_m \sum_{j=1}^{N} A_z^j(\mathbf{r}_c) - \sum_{j,k=1}^{n} C_{jk} I_j I_k\right], \tag{6.15}$$

where A_z^j is the vector potential due to the element j and $\mathbf{r}_c$ is a position inside the core. Analytical expressions for $A_z^j(\mathbf{r})$ are presented in [94].

To calculate the loss for I_m up to I_c it is necessary to know the kernel position. The kernel is defined as the last point to be penetrated by current, so that it always belongs to the field-free core for any $I_m \leq I_c$. For a $n_{f,x} \times n_{f,y}$ matrix array of strips with odd $n_{f,x}$ and $n_{f,y}$ the kernel is always located at the strip center due to mirror symmetry, although for even $n_{f,x}$ and/or $n_{f,y}$ the determination of the kernel is not so simple. Since $\mathbf{B} = 0$ always in the kernel, the kernel can be found as the point where $\mathbf{B} = 0$ inside the superconducting region when $I = I_c$. After calculating the magnetic induction generated by a saturated rectangular strip using the Biot-Savart law, the kernel position can be found numerically by means of the Newton-Raphson method for nonlinear systems of equations [95]. Due to symmetry, for matrices with either $n_{f,x}$ or $n_{f,y}$ to be even there will appear two kernels in the two strips closest to the origin, while when $n_{f,x}$ and $n_{f,y}$ are both even the system will have four equivalent kernels.

6.3 Other applications of the model

Although the critical-state model calculations of this thesis focus on infinitely long samples, like superconducting tapes, some other applications of the MEM procedure are worth to mention. These are cylinders, which can be a part of a levitating system, and granular materials like coated conductors.

6.3.1 Cylindrical geometry and levitation

As mentioned above, the MEM procedure was originally developed for finite cylinders [72, 73, 6, 96], and can therefore be directly applied to other shapes with cylindrical symmetry, such as rings. The original model was further developed for magnetic-induction-dependent critical current densities $J_c(B)$ [72, 74], which allowed a deeper study of the experimental determination of $J_c(B)$ dependence from magnetization loops [74].

The model is suitable for nonuniform applied fields $H_a(\mathbf{r})$, so that the levitation system made of a cylindrical superconductor and permanent magnet can be studied. Specifically, the model allows to calculate the levitation force [73, 97, 98], the stiffness and damping in the vertical direction [99, 100] and the lateral stiffness [101]. Moreover, this model can be extended for the levitation of hard superconductors after field cooling [102, 103].

6.3.2 YBCO coated conductors

The YBCO coated conductors consist of a superconductor thin layer grown on a metallic substrate, having some buffer layers in between. Nowadays, there is a lot of effort employed to produce and characterize this kind of conductors, since, among other reasons, the superconductor on them has a higher critical-current density than in Ag/Bi-2223 tapes. The superconducting layer on a coated conductor has a granular structure, which makes it difficult to characterize and may limit the transport current.

A possible characterization of the granularity in coated conductors can be done by means of ac susceptibility measurements for an applied field perpendicular to the wide direction. In [29] it is described a method to determine the intragrain and intergrain critical-current densities ($J_{c,\mathrm{g}}$ and $J_{c,\mathrm{b}}$, respectively) by comparing the experimental data of the ac susceptibility to the critical-state model calculations for infinitely long bars with longitudinal applied field. In [104, 105] we do a similar analysis but using 1D calculations for thin disks performed by Clem and Sanchez [89] or, when required, our MEM calculations for cylinders with finite thickness. In this way, the critical-state calculations can be compared to the experimental data for actual coated conductors, which have a high with-to-thickness aspect-ratio. Applying this analysis to measured data, we found that the intragrain contribution to χ' and χ'' is negligible due to the small grain size. However, the measured χ'' showed two peaks, which can be due to two different intergrain current densities in the samples caused by the existence of two grain-boundary main angles [105, 104]. Moreover, χ' measurements revealed the existence of domains with a size of the same order of magnitude as the whole sample.

Furthermore, we have developed a method to simultaneously measure $J_{c,\mathrm{g}}$ and $J_{c,\mathrm{b}}$ by means of magnetization loops [34]. The extraction of $J_{c,\mathrm{g}}$ and $J_{c,\mathrm{b}}$ from measured data was done assuming the critical-state model and that all the grains are cylindrical with identical dimensions. Due to the finite thickness of the grains, MEM calculations were required.

6.4 Chapter summary and conclusions

In this chapter we present a 2D numerical method to describe the electromagnetic properties of an infinitely long superconductor under a transverse applied field or a transport current, taking into account the superconductor finite-thickness effects. This method is based on the magnetic energy minimization (MEM) within the critical-state model (Sec. 2.3.3), considering a constant critical-current density. Different from conventional finite-elements methods, this numerical method implies a division into elements of the superconducting region only.

For multifilamentary superconductors under a transverse applied field we distinguish between filaments electrically isolated and those mutually interconnected at infinity. The application to the isolated case requires the restriction for the current density of zero net current inside each filament, which complicates the numerical method.

In the following chapters we apply the MEM to a single rectangular strip and regular arrays of strips submitted to a transverse ac magnetic field (chapter 7) or transport current (chapter 8).

CHAPTER 7

Superconducting tapes in transverse ac magnetic fields

Some of the important applications of superconductors are based on the possibility of having a large value of current transported through them, such as power transmission cables, magnets, transformers, and motors [106, 107, 108, 109]. For these applications, most commonly used superconductors such as $Bi_2Sr_2Ca_2Cu_3O_{10}$, $YBa_2Cu_3O_{7-\delta}$ or MgB_2 are often being set up in multifilamentary tape-shaped conductors with a metallic sheath or substrate [107, 110]. For practical reasons, it is fundamental to reduce as much as possible the transport and magnetic ac loss produced in these superconducting tapes [111, 108], which can only be done after a deep understanding of the loss nature. In this chapter we concentrate on the magnetic ac loss and the ac susceptibility in some single-filament and multifilamentary geometries, while in chapter 8 we study their transport loss.

The magnetic ac loss Q_m in multifilamentary tapes has its origin in mainly three mechanisms. They are the eddy currents in the conducting sheath, the magnetic hysteresis arising from the flux pinning in the superconductor, and the inter-filament currents (also known as coupling currents) that flow across the conducting matrix [112, 113]. Although it is somehow understood how to reduce the eddy and coupling currents loss [114, 30], important work remains to be done concerning the hysteresis loss. Many experimental works showed that the hysteresis loss depends strongly on the orientation of the external ac field [115, 116, 117]. In these studies it is shown that the hysteresis loss under an applied field H_a perpendicular to the wide face of the superconducting tapes is more than one order of magnitude higher than if H_a is either parallel to the wide face or in the transport direction.

Apart from the ac loss, another interesting quantity is the ac susceptibility, which has been shown to be a useful tool to characterize superconducting materials [29, 28, 17] and is directly related to the magnetic ac loss [29, 89].

In this chapter we study the magnetic behavior, including magnetic ac loss, due to the superconductor hysteresis under a transverse applied ac field. We consider the cases of electrically isolated strips and mutually interconnected at infinite, referred in this thesis as isolated and interconnected cases, respectively (Sec. 6.1.2). The case which presents lower magnetic ac loss is the isolated one [112, 113, 118, 38]. On the other hand, the interconnected case can describe the limiting situation of a high number of superconducting intergrowths between filaments [119, 120, 121, 122, 123] or when the coupling currents through the conducting matrix are of the same order as the superconducting currents [30, 38, 124, 125]. In order to provide a description of multifilamentary tapes, we first study the behavior of one single filament with rectangular cross-section and then we discuss the interaction between strips in several regular arrangements, such as vertical and horizontal arrays, matrices and interleaved geometry.

7.1 Previous existing results

For the rectangular strip geometry, the first calculations within the critical-state model were performed by Bean himself for a slab in [8], although analytical formulae for the magnetization curves and ac susceptibility were calculated and summarized by other authors in [28, 126]. Another interesting analytical results are the one-dimensional (1D) calculations for infinitely thin strips, performed by Brandt *et al* [87, 127, 128] and Zeldov *et al* [129]. The more general case of a strip with finite thickness was studied by Brandt using a numerical method which assumes a $E(J)$ relation as $E(J) = E_c(J/J_c)^n$ [88], which for the $n \to \infty$ limit corresponds to the critical-state model. Although Brandt presents results for current profiles, flux lines and magnetization curves, no systematic study of the ac susceptibility was done.

Concerning multifilamentary structure, one of the most interesting results within the critical-state model are those obtained by Mawatari for a infinite set of strips periodically arranged in the vertical and horizontal directions for the thin-strip limit [92, 130]. Another important analytical calculations within the critical-state model are those for a double thin strip, obtained by Ainbinder and Maksimova [131]. Moreover, Fabbricatore *et al* performed numerical calculations for the complete-shielding state in vertical, horizontal and matrix arrays of strips, as well as realistic cross-sections for multifilamentary tapes [68, 69]. Other numerical calculations have been done by assuming a $E(J) = E_c(J/J_c)^n$ dependence. This is the case of Tebano *et al* [132], who applied the Brandt's method to vertical stacks. Moreover, Stavrev *et al* performed numerical calculations by means of a conventional finite-elements method for multifilamentary tapes [133, 134], although they did not consider the most important case of isolated strips. In spite of the above calculations, the case of a set of rectangular strips in the critical-state model has not been systematically studied, specially for the isolated case. The object of this chapter is to cover this lack.

7.2 Single rectangular strip

In this section we concentrate in ac susceptibility calculations, since current profiles and magnetic flux lines were already calculated by Brandt in [88], although they correspond to a $E(J)$ dependence as $E(J) = E_c(J/J_c)^n$ instead of the critical-state model. An extended version of this section is presented in [85].

7.2.1 Analytical limits

First, we present some interesting analytical limits which we will use in the following sections.

Low-field limit

The application of a very low field (approaching zero) to a zero-field cooled superconducting bar will induce critical supercurrents flowing in a very thin surface layer so that the bar is shielded from the applied field. In this case, the material can be taken as LHI with internal susceptibility $\chi = -1$, so that the external complex ac susceptibility is real with $\chi' = \chi_s^*$, being χ_s^* the shape susceptibility (§3.3). Its absolute value, $\chi_0 = -\chi_s^*$ is usually called the initial susceptibility, since it corresponds to the magnitude of the slope of the initial magnetization curve for $H_a \to 0$. As presented in Sec. 3.3, the shape susceptibility is related to the magnetometric demagnetizing factor as

$$\chi_s^* = -\chi_0 = [1 - N_m(\chi = -1)]^{-1}. \tag{7.1}$$

Then, χ_0 can be found analytically from the expression for $N_m(\chi = -1, a/b)$ obtained in Sec. 4.1.3 (Eq. (4.33)). The deduced analytical formula for χ_0 is therefore

$$\chi_0 = \frac{\pi k'^2}{4[E(k) - k'^2 K(k)][E(k') - k^2 K(k')]}, \tag{7.2}$$

$$\frac{a}{b} = \frac{E(k') - k^2 K(k')}{E(k) - k'^2 K(k)}, \tag{7.3}$$

$$k'^2 = 1 - k^2, \tag{7.4}$$

where K and E are the complete elliptic integrals of the first and second kind and k and k' are their modules. From Eq. (7.1) and Fig. 4.3(b), we see that χ_0 monotonically decreases with increasing b/a, approaching 1 at high b/a, which is logical since demagnetizing effects are very weak in this case. The initial susceptibility approaches the thin strip limit obtained by 1D calculation [87, 127] with decreasing b/a, $\chi_0 = \pi a/(4b)$. Comparing to the exact analytical formula of Eq. (7.2), the thin strip limit involves a quite large negative error if b/a is not very small, being -3.8% and -21.1% at $b/a = 0.01$ and 0.1, respectively.

Full penetration field

Besides χ_0, another quantity that can be analytically calculated is the full penetration field H_p (Sec. 2.3.3). Since H_p is balanced at $x = y = 0$ by the field produced by supercurrents whose density $J = J_c$ at $-a \leq x \leq 0$ and $-J_c$ at $0 \leq x \leq a$, it can be calculated directly using the Biot-Savart law as done in [135, 88]

$$H_p = \frac{J_c b}{\pi}\left[\frac{2a}{b}\arctan\frac{b}{a} + \ln\left(1+\frac{a^2}{b^2}\right)\right]. \tag{7.5}$$

We note that this equation is valid for any b/a aspect ratio, including the low-b/a limit.

Other existing limits

The ac susceptibility for an infinite slab, corresponding to the high-b/a limit, has been analytically derived in [28] from the Bean's formulae for the magnetization loop [8].

If b/a is very low, χ' and χ'' may be calculated using Eqs. (6.5), (6.7) and (6.8), from the initial magnetization curve of a thin strip obtained by 1D calculations [87, 127, 129],

$$M_i(H) = -\frac{\pi a H_c}{4b}\tanh\frac{H}{H_c}, \tag{7.6}$$

as

$$\frac{\chi'}{\chi_0} = \frac{4H_c}{\pi H_m}\int_0^{\pi}\tanh\left[\frac{H_m}{2H_c}(1-\cos\theta)\right]\cos\theta\,\mathrm{d}\theta, \tag{7.7}$$

$$\frac{\chi''}{\chi_0} = \frac{4H_c}{\pi H_m}\left(\frac{2H_c}{H_m}\ln\cosh\frac{H_m}{H_c} - \tanh\frac{H_m}{H_c}\right), \tag{7.8}$$

where $\chi_0 = \pi a/4b$ and $H_c = 2J_c b/\pi$.

7.2.2 Numerical results and discussion

When the amplitude of the ac field is not very small, the current density penetrates in the superconductor and the perfect shielding approximation is no longer valid. For the limits of slabs ($b/a \to \infty$) and thin strips ($b/a \to 0$) the whole curves for $\chi'(H_m)$ and $\chi''(H_m)$ in the critical-state model can be analytically derived, as done in [28] and [87, 127, 129] for slabs and thin strips, respectively. However, for the more realistic case of finite b/a no analytical formulae nor numerical calculations for the $\chi'(H_m)$ and $\chi''(H_m)$ curves have been found.

To fill this gap, here we present accurate numerical calculations obtained by means of the MEM procedure. All the numerical calculations for rectangular strips are performed with a maximum of 72000 elements, which correspond to $n = 36000$ circuits, and a number of current steps $10 \leq m_m \leq 40$, increasing with decreasing H_m and increasing b/a. The use of these parameters allows to obtain highly accurate results.

Susceptibility versus field

In Fig. 7.1 we plot the normalized real, χ'/χ_0, and imaginary, χ''/χ_0, parts of the ac susceptibility as a function of the normalized field amplitude H_m/H_p for an infinitely long rectangular strip with cross-section $2a \times 2b$ and ac applied field in the b direction. In this figure we present the results for some b/a aspect ratios, while a table containing data for more b/a values can be found in [85].

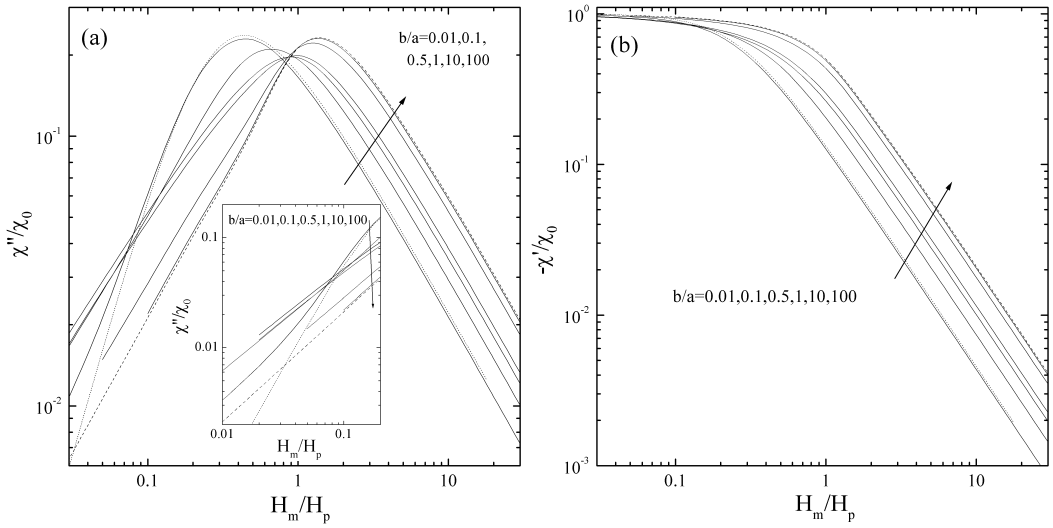

Figure 7.1: Numerically calculated χ''/χ_0 (a) and $-\chi'/\chi_0$ (b) as functions of H_m/H_p for $b/a = 0.01, 0.1, 0.5, 1, 10$, and 100 (solid lines). The dotted and dashed lines are those for the analytically calculated results for a thin strip [Eqs. (7.7) and (7.2.1)] and for the an infinite slab ($b/a \to \infty$) [28]. For the curves of the 1D thin strip, H_c is converted to H_p at $b/a = 0.01$, using $H_c = 2J_c b/\pi$ and Eq. (7.5).

From the $\chi'/\chi_0(H_m)$ and $\chi''/\chi_0(H_m)$ curves in Fig. 7.1, we can see that for high fields χ'/χ_0 and χ''/χ_0 decrease as H_m^{-1} and $H_m^{-3/2}$, respectively. These limits were also found for infinitely long rectangular strips in longitudinal applied fields [29]. The behavior of χ'' at high fields can be easily understood taking into account that χ'' is proportional to the area of the hysteresis loop (or ac loss),

$$\chi''(H_m) = \frac{1}{\pi H_m^2} \oint M \mathrm{d}H_\mathrm{a}. \tag{7.9}$$

For constant J_c at high H_m, the main part of the loop consists of two horizontal lines determined by fully penetrated constant critical-state magnetizations. Thus, $\oint H\mathrm{d}M \propto H_m$ roughly and we have $\chi'' \propto H_m^{-1}$ roughly from Eq. (7.9). This is a universal feature for the critical-state model with constant J_c and does not depend on the cross-section geometry.

Since intuitively a rectangular bar of $b/a = 0.01$ should be well approximated by the 1D model of thin strip, we have compared the results of 2D numerical and 1D analytical

calculations for $b/a = 0.01$ in Figs. 7.1(a) and (b). In this figure we can see that the χ''/χ_0 for the 1D results are slightly higher than those for the 2D calculations for $H_m/H_p \geq 0.2$, being the difference 2.8% to 3.9% at $H_m/H_p = 0.5$ to 100. This trend is reversed for $H_m/H_p \leq 0.2$, being the 1D calculation results lower with the difference increasing with decreasing H_m. Moreover, for very low fields, $H_m/H_p \leq 0.01$, the 1D results decrease as H_m^2 with decreasing H_m, while 2D ones decrease as H_m. Concerning $-\chi'/\chi_0$, the 1D results are greater than the 2D ones for 4.3% to 4.8% at $H_m/H_p = 0.5$ to 100, whereas at low H_m/H_p, the value of $1 + \chi'/\chi_0$ increases in proportion to H_m and H_m^2 for 2D and 1D calculations, respectively.

In order to understand the above differences, we first consider the 1D strip and the infinite slab. As derived by Norris [86], applying a small ac field to a zero-field cooled hard superconductor with constant J_c, if the penetration depth δ at $H = H_m$ is uniform over the surface, the loop area $\oint M\mathrm{d}H$ will be proportional to $\Phi\delta$, where Φ is the average flux between the penetrated layer and a field-free core. Using this rule and Eq. (7.9), we can explain the low-field $\oint M\mathrm{d}H \propto H_m^4$ and $\chi'' \propto H_m^2$ of 1D strip from $\delta \approx a(H_m/H_c)^2/2$ and $\Phi \approx a\mu_0 H_m^2/2H_c$ [87, 127]. For the case of infinite slab, $b/a \to \infty$, we can easily obtain $\delta = aH_m/H_p$ and $\Phi \approx a\mu_0 H_m^2/4H_p$, so that $\oint M\mathrm{d}H \propto H_m^3$ and $\chi'' \propto H_m$ at low H_m. The main difference between both cases occurs in δ, which is proportional to H_m for the slab with planar penetration fronts but to H_m^2 for the strip with linear penetration fronts. For intermediate b/a, current profiles also penetrate as $\delta \propto H_m$ for low applied fields. This is so because the current penetration for low applied fields is proportional to the surface current density in the complete-shielding state [113, 136, 137, 138, 91] which, at the same time, is proportional to the applied field. Consequently, in the critical-state model with constant J_c, χ'' for any geometry must be proportional to H_m in the low-H_m limit.

Peak in the $\chi''(H_m)$ curve

The most important issue in the χ''/χ_0 versus H_m/H_p curve is the presence of a peak at a certain ac amplitude $H_{m,\mathrm{pk}}$, having a height χ''_{pk}. The numerical results for $\chi''_{\mathrm{pk}}/\chi_0$ and $H_{m,\mathrm{pk}}/J_c a$ are plotted in Figs. 7.2(a) and 7.2(b), respectively. Since the discrepancy between $H_{m,\mathrm{pk}}$ and H_p is a remarkable feature, we plot $H_{m,\mathrm{pk}}/H_p$ as a function of b/a in Fig. 7.2(c). In Figs. 7.2(b,c) we also plot the analytical limits for a thin strip and a slab, which are

$$\chi''_{\mathrm{pk}}/\chi_0 \approx 0.2365, \tag{7.10}$$

$$H_{m,\mathrm{pk}}/J_c a \approx 1.569 b/a, \tag{7.11}$$

$$H_{m,\mathrm{pk}}/H_{\mathrm{p}} \approx 2.464/\ln(ea/b) \tag{7.12}$$

for the thin strip [85, 87, 127] and

$$\chi''_m/\chi_0 = 3/4\pi \approx 0.2387, \tag{7.13}$$

$$H_{m,\mathrm{pk}}/J_c a = H_{m,\mathrm{pk}}/H_{\mathrm{p}} = 4/3 \approx 1.333 \tag{7.14}$$

for the slab [28].

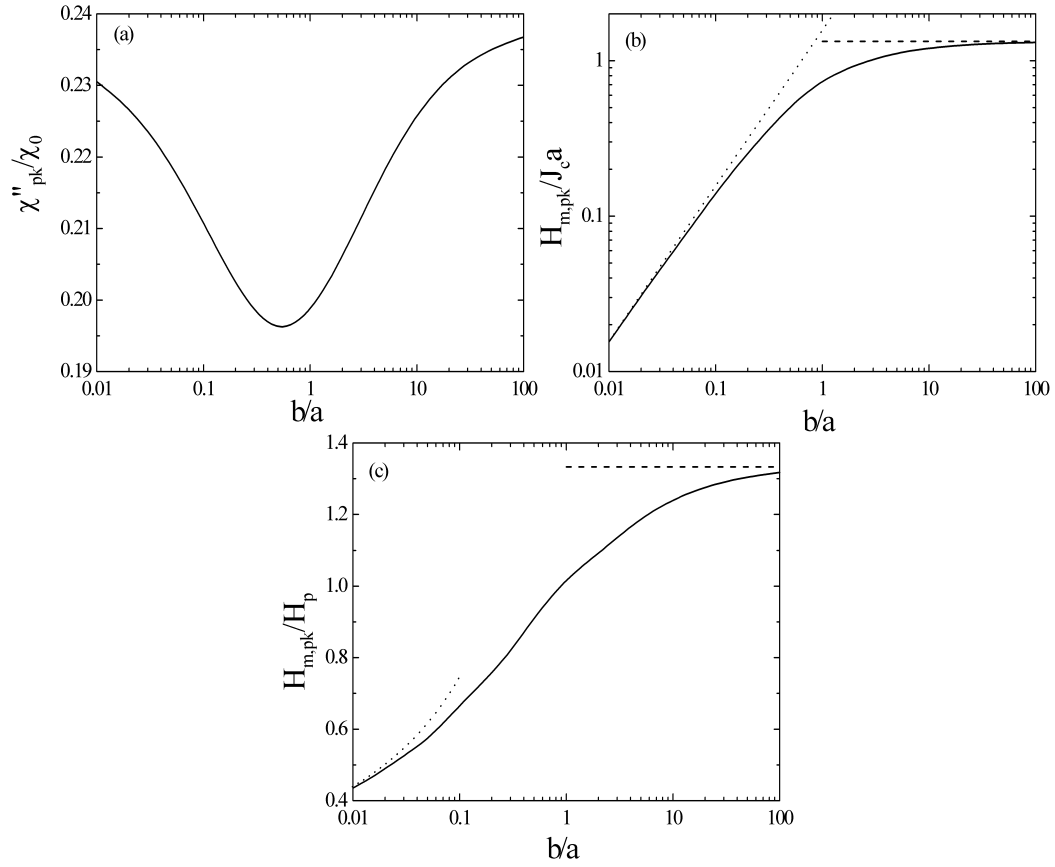

Figure 7.2: (a) Numerically calculated $\chi''_{\rm pk}/\chi_0$ as a function of b/a. (b) Numerically calculated $H_{m,\rm pk}/J_c a$ as a function of b/a (solid line) compared with its low (dotted line) and high-b/a (dashed line) limits calculated using Eqs. (7.11) and (7.14). (c) Numerically calculated $H_{m,\rm pk}/H_p$ as a function of b/a (solid line) compared with its low (dotted line) and high-b/a (dashed line) limits calculated using Eqs. (7.12) and (7.14).

For the studied rectangular bar with constant J_c in a transverse field, with decreasing b/a from ∞ to 1, $\chi''_{\rm pk}/\chi_0$ decreases from 0.239 to 0.199 and $H_{m,\rm pk}/H_p$ decreases from 1.33 to 1.01. This is quite similar to the case of the same bar in a longitudinal field, where $\chi''_{\rm pk}/\chi_0$ decreases from 0.239 to 0.212 and $H_{m,\rm pk}/H_p$ decreases from 1.33 to 1, with decreasing b/a from ∞ to 1 (further decreasing b/a will repeat the result at a/b). However, with further decreasing b/a from 1 to 0.01, the transverse $\chi''_{\rm pk}/\chi_0$ undergoes a minimum value of 0.196 at $b/a \approx 0.5$ and then increases to 0.231, and $H_{m,\rm pk}/H_p$ decreases from 1.01 to 0.434. It is not easy to make accurate numerical 2D calculations at even smaller b/a, but we can roughly use the results of 1D calculation at intermediate H_m/H_p to expect that the low-b/a limit of $\chi''_{\rm pk}/\chi_0$ is 0.237 and the $H_{m,\rm pk}/H_p$ will decrease logarithmically with decreasing b/a (Eq. (7.12)), being 0.2 and 0.1 at $b/a \approx$

0.001 and 0.00001.

As long as the assumption of critical-state model with constant J_c is suitable for actual samples, the $H_{m,\mathrm{pk}}/J_c a$ calculations can be used to experimentally determine J_c in a nondestructive way by measuring $H_{m,\mathrm{pk}}$. For this reason, we present tables of $H_{m,\mathrm{pk}}$ for several b/a in [85]. A similar table for elliptical tapes and cylinders can be found in Refs. [33] and [104], respectively. For elliptical tapes, we found a good agreement to actual experimental data [32, 33]. In addition, in the initial magnetization curve, M saturates at $H_\mathrm{a} = H_p$, although for samples with low b/a, M apparently saturates at an applied field much lower than H_p (Fig. 7.3). However, $H_{m,\mathrm{pk}}$ agrees well to the apparent saturation field for $b/a \leq 1$, being M at this field higher than 98% of the saturated value for any b/a. This issue has been used to determine the inter-granular J_c for actual YBCO coated conductors in [34].

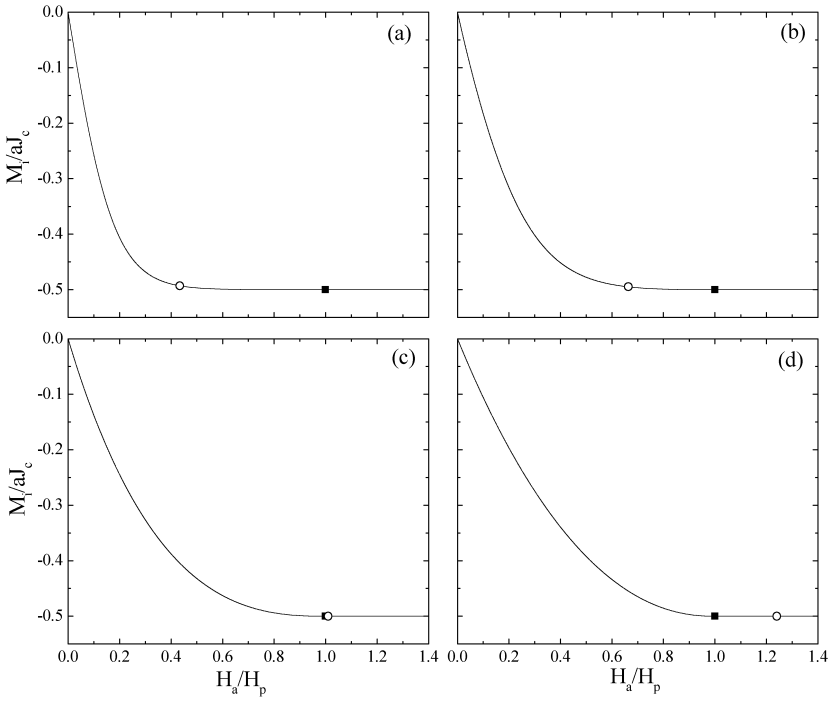

Figure 7.3: Initial magnetization curves for rectangular strips as a function of H_a/H_p for $b/a = 0.01$ (a), 0.1 (b), 1 (c) and 10 (d). Open circles are for $M_i(H_\mathrm{a} = H_{m,\mathrm{pk}})$, while solid squares are for $M_i(H_\mathrm{a} = H_p)$.

7.3 Vertical stacks

Up to this point, we have thoroughly studied the geometry of one single strip. We shall next study the effects of the magnetic interaction between rectangular strips. In this section, we start by studying the case of rectangular strips arranged linearly in the

direction parallel to the applied field with a constant strip separation d_y (see inset in Fig. 7.5), which is a geometry commonly found in practice. Below we shall deal with the cases of horizontal arrays and matrix configurations.

The calculations presented in sections 7.3, 7.4 and 7.5 are done using between 22000 and 60000 elements in the total cross-section, which corresponds to 1300 $\sim$ 20000 elements per strip with $m_m = 1$ (the number of elements per strip is lower for arrays with more strips). All the numerical calculations in Secs. 7.3, 7.4 and 7.5 are presented in [71, 70, 139] and have been performed before the MEM procedure with steps in J_c was developed, introduced in [84]. This, together with the fact that we have to use a lower number of elements per strip, are the reasons for the lower accuracy obtained as compared to the results in Sec. 7.2.

7.3.1 Current profiles and magnetic flux lines

The most important issue to study in the system of superconducting strips is the influence of magnetic coupling. To study this effect we present in Fig. 7.4 calculations corresponding to a vertical stack of three strips with $b/a = 0.1$ and different separations ($d_y = 2a$, $d_y = 0.2a$, and $d_y = 0.02a$ for Figs. 7.4(a), (b) and (c), respectively). The depicted situation corresponds to an applied field of $H_a/H_p = 0.4$, where H_p is the field at which the array is fully penetrated by current (such a field is calculated analytically in [71]). The results show unambiguously the strong influence of magnetic coupling in the case that the separation is small, as illustrated in the case for $d_y = 0.02a$ for which the current profile is almost the same as if there were no gaps between the strips. For the other extreme, the case $d_y = 2a$ is already an example of a very weak magnetic coupling that results in a current penetration for each strip almost as if the two others were not present.

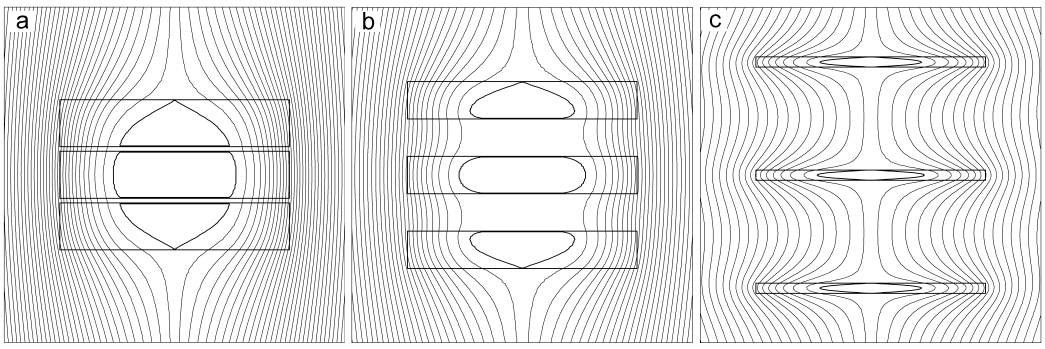

Figure 7.4: Magnetic flux lines and current profiles (thicker lines) corresponding to an applied field H_a/H_p=0.4, where H_p is the penetration field of the vertical stack, for a three-strip vertical stack with $b/a = 0.1$ and $d_y/a = 2$ (a), 0.2 (b), and 0.02 (c). Vertical and horizontal dimensions are not in scale. Flux lines for all cases correspond to the same vector potential difference.

It is clear that for $d_y = 0.02a$ and even $d_y = 0.2a$, the applied field in the space

between superconductors is basically shielded by them, in contrast with the case of $d_y = 2a$, for which the magnetic field is modified near each strip but not enough to make a significant contribution to the other two. When the separation is large the total field lines created by the current are wrapped around each strip, whereas when the separation decreases up to $d_y/a = 0.02$ the field lines are hardly distinguishable from the case of the three strips forming a single thicker one.

7.3.2 Magnetization

In this section we analyze the magnetization of the vertical stacks, calculated from the currents following Eq. (2.1). The reverse and returning curve can be obtained from the initial one using Eqs. (6.5) and (6.6). There are several important properties of the arrays that can be understood from the magnetization results.

Dependence on strip separation

In Fig. 7.5 we plot the calculated initial magnetization curve $M_i(H_a)$ for a vertical stack of three strips, each with semisides ratio b/a of 0.01 and with different separations $d_y/a = 0.02, 0.2$, and 2, respectively. We also plot the curve for a single strip with $b/a = 0.01$ and another one for $b/a = 0.03$, corresponding to the case that the three strips are one on top of each other.

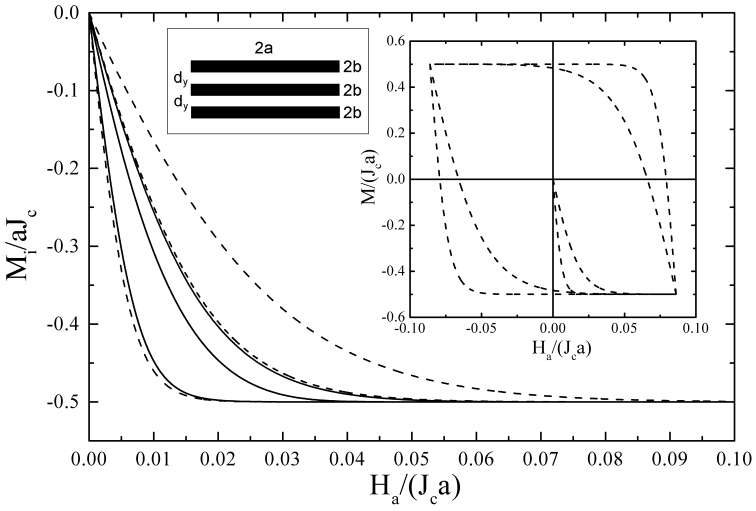

Figure 7.5: Initial magnetization as a function of the applied field. Dash lines are for single rectangular strips with $b/a = 0.01$, 0.03 and 0.05 from left to right. Solid lines correspond to a three-strip vertical stack with $b/a = 0.01$ and separation $d_y/a = 2$, 0.2 and 0.02 from left to right. In the inset complete magnetization loops are plotted for strips with $b/a = 0.01$ and 0.03.

One can observe in Fig. 7.5 that the saturation magnetization remains the same for all cases, whereas the initial slope of the magnetization curve, with magnitude χ_0,

changes. The initial slope and the magnetization below the penetration field monotonically increase in magnitude with increasing d_y, approaching the curve for a single strip with $b/a = 0.01$ and that with $b/a = 0.03$ for the high d_y and low d_y limits, respectively.

The reason for the enhancement of χ_0 with decreasing d_y is the demagnetizing effect associated with the sample aspect ratio, according to which the thinner the sample, the larger χ_0 (§7.2.1) [85, 88, 72]. In the arrays for which d_y is small, there is a strong magnetic coupling between strips (see Fig. 7.4) so that the whole sample is behaving as a single strip with larger thickness than for one of the strips of the stack, thus presenting lower χ_0. In order to study in more detail this effect, we have included in Fig. 7.5 the calculated magnetization of a single strip with $b/a = 0.05$; this strip corresponds to the array with $d_y/a = 0.02$ but as if the gaps between the strips were filled by superconducting material as well. We can see that this case has the smallest slope, and there are large differences with respect to the case of the array of three strips with separation $d_y/a = 0.02$.

Then, the magnetic properties of a vertical stack of $n_{f,y}$ strips close together are similar to those for a strip, which we call the equivalent strip, with aspect ratio $n_{f,y}b/a$.

Dependence on the number of strips

Another interesting feature to study is the effect of adding more strips to the array. We compare in Fig. 7.6 the calculated $M_i(H_a)$ curves for arrays with a fixed distance ($d_y = 0.2$) and different number of strips. We include in the figure the two known analytical limits of one infinitely thin strip [87, 127, 129] and for an infinite stack of thin strips [92] since, as discussed in Sec. 7.2.2, there is a good agreement between 1D calculations and 2D ones for thin strips, provided that H_m is not very small. With adding more strips, χ_0 gets smaller. We find that even the case of 25 strips is significantly different from the Mawatari case for an infinite stack, so we can conclude that Mawatari's formula should be valid only for a very large number of strips. Calculations for the same vertical stacks with larger d_y, $d_y/a = 2$, showed that the change in the $M_i(H_a)$ curve due to the variation of $n_{f,y}$ is smaller, owing to a lower magnetic coupling among the strips [71].

7.3.3 χ'' calculations

In this subsection we focus on the imaginary part of the ac susceptibility χ'', since it is directly related to the magnetic hysteresis ac loss in the tape [Eq. (6.9)]. The real part of the ac susceptibility is not presented for the sake of brevity.

Dependence on strip separation

We present in Fig. 7.7 the calculated results for χ'' as function of the ac applied field amplitude H_m corresponding to the magnetization curves of Fig. 7.5. Same as for a single strip, Sec. 7.2.2, the $\chi''(H_m)$ curves show a peak, which corresponds to a change

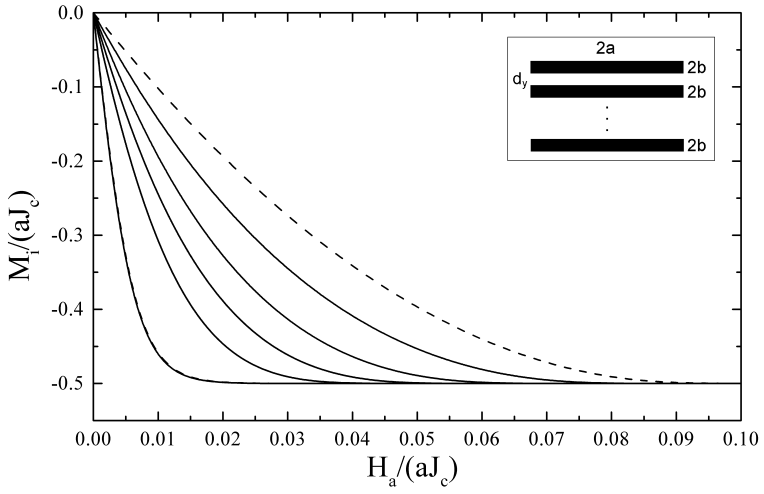

Figure 7.6: Initial magnetization as a function of the applied field. Solid lines are for vertical stacks of strips with $b/a = 0.01$ and $d_y/a = 0.2$ composed of 1, 3, 5, 9 and 25 strips from left to right. Dash lines are for the 1D analytical limits of a thin strip of Eq. (7.2.1) with $b/a = 0.01$ (almost overlapped with the corresponding 2D calculation) and for a vertical infinite array of thin strips with $b/a = 0.01$ and $d_y/a = 0.2$ [92, 130] (upper curve).

in slope of the ac loss, since they are proportional to χ'' times $H_{\rm m}^2$, Eq. (6.9). It can be seen that the peak in χ'' is shifting to higher fields and decreasing in magnitude with decreasing the separation distance. This feature can be understood from the decrease in magnitude of the $M_i(H_{\rm a})$ curve for $H_{\rm a} < H_p$ (Fig. 7.5) and the relation between χ'' and the magnetization loop [Eq. (6.8)]. As explained in Sec. 7.3.2, the key factor that characterize the $M_i(H_{\rm a})$ curves is χ_0, which is governed by the demagnetizing effects.

Results in Fig. 7.7 show that the $\chi''(H_m)$ curve for low ac fields decreases as $(H_m)^n$ with decreasing H_m, being n between 1.5 and 1.3. However, for even lower H_m we expect a decrease of the n exponent down to 1, as it is the case of a rectangular strip with $b/a = 0.01$ (Fig. 7.1). According to the discussion in Sec. 7.2.2, in the critical-state model with constant J_c the low-H_m limit $\chi'' \propto H_m$ must appear for any 2D cross-section, whether it is multifilamentary or not. For high fields, χ'' goes as H_m^{-1} for all cases, as it is general for the critical-state model (Sec. 7.2.2) [29, 85]. Moreover, for this limit all curves converge to a single one, since $\chi'' \propto M_s/H_m$, Eq. (7.9), and M_s does not depend on d_y.

Dependence on the number of strips

In Fig. 7.8 we calculate the results for χ'' as function of H_m with the goal of studying the effect of adding more strips in the array. We use the same cases as in Fig. 7.6, corresponding to $d_y/a = 0.2$ and several $n_{f,y}$ values. Again, there is a close relation between the increase in χ_0 and the saturation field and the corresponding increase of $\chi''_{\rm pk}$ and $H_{m,{\rm pk}}$, respectively. It is interesting to comment, however, that the formulae

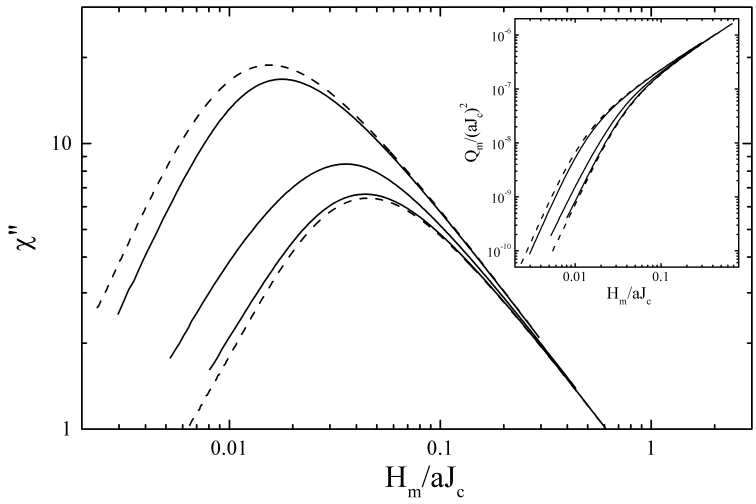

Figure 7.7: Imaginary part of the ac susceptibility χ'' as a function of the ac field amplitude $H_{\rm m}$ corresponding to the curves of Fig. 7.5, in the same order (the case of a single strip with b/a=0.05 is not plotted in this figure). The corresponding power loss is shown in the inset.

provided by Mawatari for the case of an infinite array are not adequate to describe quantitatively the ac loss of a finite array even if the array consists of up to 25 strips.

From the calculations presented in this section we find that in order to reduce Q_m in a real superconducting tape with a vertical stack geometry one should increase the coupling of the filaments by decreasing the strip distance (see Fig. 7.7). Also, the results in Fig. 7.8 show that, keeping the distance between strips, Q_m decreases with increasing $n_{f,y}$, particularly in the case of a small strip separation ($d_y/a = 0.2$, Fig. 7.8).These results can be understood as follows. With decreasing d_y from ∞ to 0, the array progressively changes from behaving as uncoupled strips with aspect ratio b/a to act as a single superconducting tape with aspect ratio $n_{f,y}b/a$, so the demagnetizing effects decrease, χ_0 is lower (Sec. 7.2.1), and so is the area of the hysteresis loop for a given H_m yielding to a reduction of the ac loss.

It is interesting to notice that when we talk about the separation d_y being small one should understand it small as compared to the horizontal dimension $2a$ and not to the strip thickness $2b$. Calculations of the same values of d_y/a for the case $b/a = 0.1$ (instead of $b/a = 0.01$ as in the results presented above), for example, yield qualitatively the same effects for the same d_y/a values.

7.4 Horizontal arrays

We now present the current profiles, magnetic field lines $M_i(H_{\rm a})$ and $\chi''(H_m)$ for linear arrays of strips arranged in the direction perpendicular to the applied field with uniform separation d_x (see inset in Fig. 7.5).

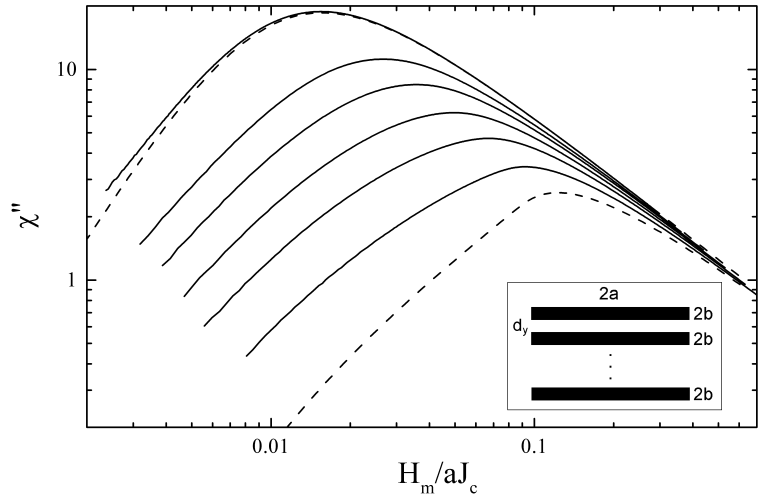

Figure 7.8: Imaginary part of the ac susceptibility χ'' as a function of the amplitude of the ac field $H_{\rm m}$ corresponding to the curves of Fig. 7.6, in the same order.

7.4.1 Current profiles and magnetic flux lines

For the sake of clarity, we present separately the results for interconnected and isolated strips.

Interconnected strips

We first discuss the current profiles and magnetic flux lines calculated for a horizontal array composed of three strips with aspect ratio $b/a = 0.1$. In Figs. 7.9(a,c,e) we show the current profiles and the magnetic flux lines corresponding to three horizontal arrays with several d_x. The applied field in all cases is $0.2H_p$, being H_p the penetration field for the whole horizontal array [71]. For all cases, the supercurrent density is induced not only to shield the superconductors as much as possible (field is zero in the current-free regions inside the superconductors) but also the space between them. Actually, we find that there appears a small overshielding near the inner edge of the external strips (Fig. 7.9(e)), so that the field there is opposite to the applied field. This feature also appears for rings in the critical state [140] and for completely shielded toroids [141].

Isolated strips

We now present the results calculated for isolated strips case so that current has to go and return always through the same filament. We calculate the case of a three-strip horizontal array with $b/a = 0.1$ and $d_x/a = 0.02, 0.2$ and 2 if Figs. 7.9(b), (d) and (f), respectively, under an applied field of magnitude $0.1H_p$. We note that these current profiles and flux lines for isolated strips are strongly different from those for interconnected ones, Fig. 7.9.

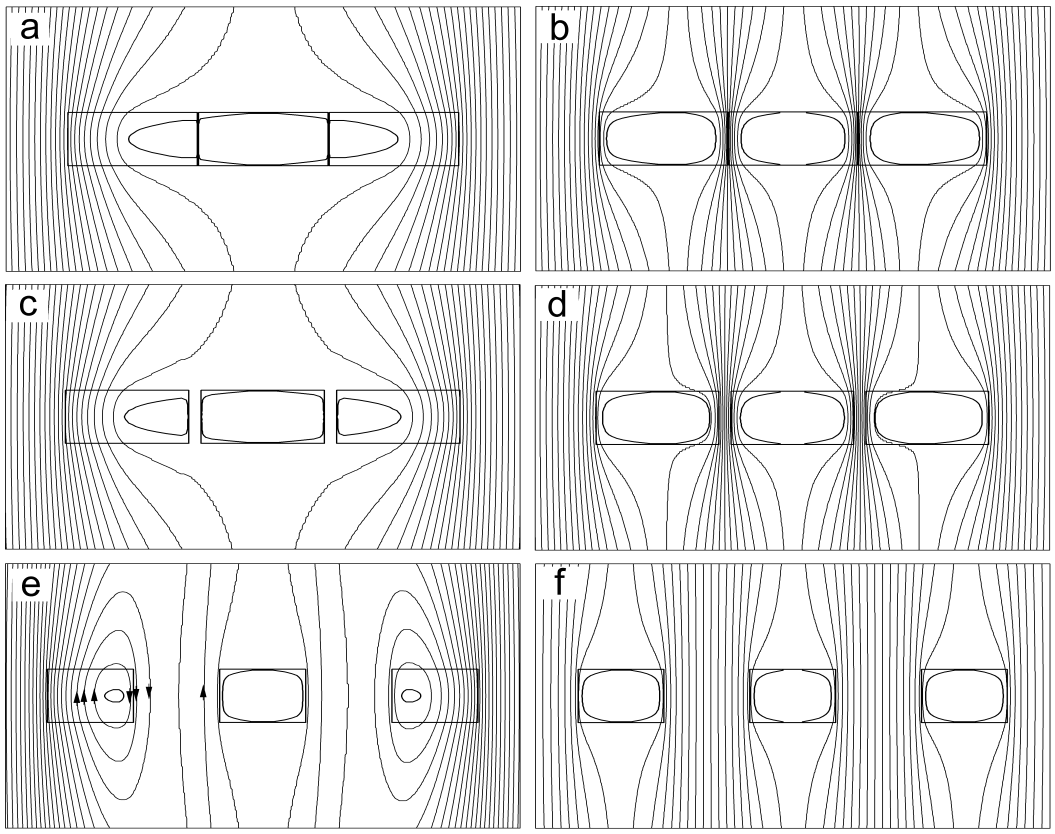

Figure 7.9: Magnetic flux lines and current profiles (thicker lines) for a three-strip vertical stack with $b/a = 0.1$ and $d_x/a = 0.02$ (a,b) 0.2 (c,d) and 2 (e,f). Left figures (a,c,e) are for interconnected strips immersed in an applied field H_a/H_p=0.2, while right ones (b,d,f) are for the isolated-strips case with an applied field of H_a/H_p=0.1. Vertical and horizontal dimensions are not in scale.

In the present case of isolated strips there is an appreciable current density penetration in all the strips and not only in the outer ones, although the magnetic coupling between them makes the current distribution in the outer strips different from the central one for smaller d_x. Another remarkable effect is that there is an important flux compression in the space between strips. Since all strips tend to shield the magnetic field in their interiors independently, the magnetic field in the air gap between each pair of strips is stronger because of the flux exclusion in both adjacent strips. Actually, flux lines are very dense not only in the gap between strips but also in the zone in the strips nearest to the gap, where current density penetrates an important distance (this effect is particularly clear for $d_x/a = 0.02$ in Fig. 7.9(b)). This flux compression effect in the critical-state model was also found by Mawatari for infinite horizontal arrays of thin strips [92] and by Ainbinder and Maksimova for a double thin strip [131]; in the completely shielding state, flux compression was found by Brandt *et al* for double

thin strips [142] and rings with zero net current [143], and by Fabbricatore *et al* for completely shielding horizontal arrays, matrices and realistic shapes of multifilamentary tapes [68, 69].

In order to compare the isolated and the interconnected cases, we plot in Fig. 7.10 the current profiles for a three-strip horizontal array with $b/a = 0.1$, $d_x/a = 0.2$ and $H_a = 0.1$, 0.2, 0.4, 0.6, 0.8 and 1 in units of H_p for each case. For interconnected strips we see in Fig. 7.10(a) that the current density penetrates from external strips to inner ones in such a way that current density is positive for $x > 0$ and negative for $x < 0$. However, for isolated strips, Fig. 7.10(b), the net current for each strip is null and current profiles are almost symmetric to each strip central vertical plane, although there is a slightly deeper penetration near the gaps. By additional calculations for other b/a values we found that this effect is enhanced with increasing b/a.

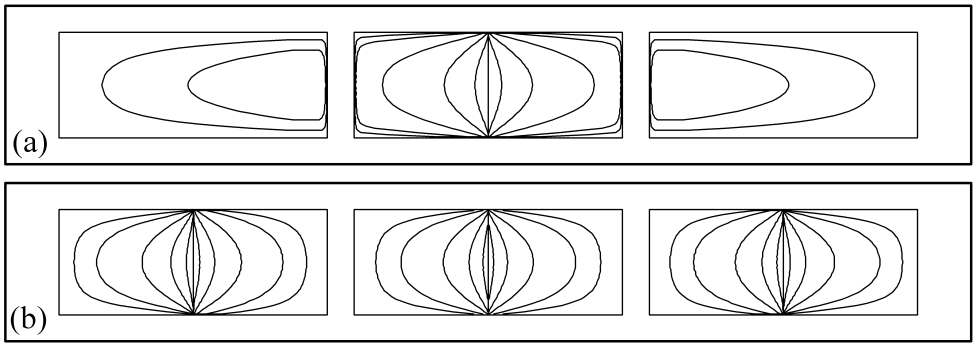

Figure 7.10: Current profiles for horizontal arrays with $b/a = 0.1$ and $d_x/a = 0.2$ for (a) interconnected strips and (b) isolated strips. The vertical scale has been expanded for clarity. The applied field values corresponding to each current profile are H_a =0.1, 0.2, 0.4, 0.6, 0.8 and 1 in units of the penetration field H_p for each case.

7.4.2 Magnetization

We now analyze the results for the magnetization of the horizontal arrays. In Fig. 7.11 we plot the calculated $M_i(H_a)$ curves for the 3 horizontal arrays of Fig. 7.9(a,c,e), corresponding $b/a = 0.1$ and $d_x = 0.02, 0.2$ and 2. The upper figure shows the results for the isolated strips whereas the data in the bottom part is for interconnected ones.

The magnetization for both isolated and interconnected strips shows important differences, arising from the different current penetration profiles studied in Sec. 7.4.1. We first discuss the results for isolated strips. It can be seen that the magnetization at saturation, M_s, does not depend on the strip separation and has a value $M_s = aJ_c/2$, which is the same as for a single strip. This is so because at saturation the $\pm J_c$ interface is a vertical straight line (Fig. 7.10). With increasing d_x up to 2, the $M_i(H_a)$ curve approaches to that for a rectangular strip with $b/a = 0.1$, corresponding to the magnetically uncoupled strips limit. We find that χ_0 increases with decreasing separa-

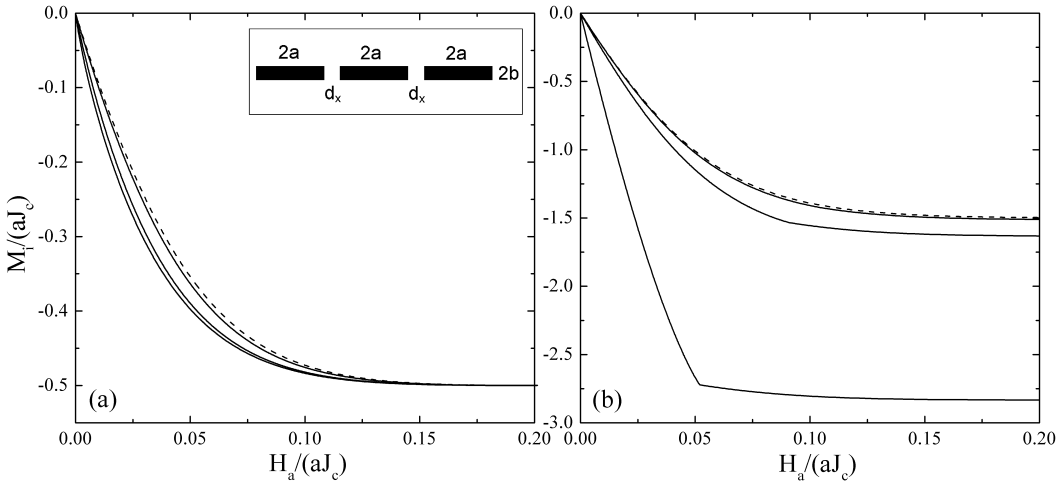

Figure 7.11: Initial magnetization curves $M_i(H_\mathrm{a})$ for horizontal arrays with three strips with $b/a = 0.1$ and several strip separations d_x/a for the cases of (a) isolated strips and (b) interconnected strips. For graph (a) solid lines correspond to horizontal arrays with d_x/a =2, 0.2, and 0.02 from top to bottom, while the dashed line represents $M_i(H_\mathrm{a})$ for a single strip with $b/a = 0.1$. For graph (b) solid lines correspond to horizontal arrays with d_x/a =0.02, 0.2, and 2 from top to bottom and the dashed line is for a single strip with halfwidth $a' = 3a$ and $b = 0.1$.

tion. The enhancement of the initial slope can be explained by the fact that the strips have to shield not only the external applied field but also the field created by the other ones. This enhancement of χ_0 have already been predicted in other related situations [92, 68, 69, 121]. Moreover, χ_0 for the low-d_x/a limit for isolated strips tends to the value for the overall. This is so because for low H_a we can take the complete shielding approximation, so that currents flow on the surface only. Then, for the $d_x \to 0$ limit the net effect of the surface current bordering the gaps cancels and χ_0 for the array is the same as for a wider strip with aspect ratio $b/(n_{f,x}a)$.

We have found that the initial slope for isolated strips calculated with our approach is coincident, within a 4% difference, with that calculated numerically by finite elements by Fabbricatore et al [68] for the case of 5×5 and 5×3 filament matrices with complete shielding.

When comparing the results for isolated strips to the case of interconnected ones, important differences appear. A first difference is that M_s in the latter case is not only larger in general with respect to the isolated case but also depends on the strip separation. For interconnected strips, the magnetization reaches the saturation value when the array is fully penetrated by currents. Since J_c is constant and current density in the $x > 0$ and in $x < 0$ is negative and positive, respectively, M_s can be easily calculated by means of Eq. (2.1) for the magnetic moment, obtaining

$$M_s = \frac{J_c a}{2}\left[1 + \frac{d_x}{2a}\right] n_{f,x} \qquad (n_{f,x} \text{ even}) \tag{7.15}$$

$$M_s = \frac{J_c a}{2}\left[n_{f,x} + \frac{d_x}{2a}\left(n_{f,x} - \frac{1}{n_{f,x}}\right)\right] \quad (n_{f,x} \text{ odd}). \tag{7.16}$$

These results are in agreement with the calculated curves in Fig. 7.11(b), which increase with increasing d_x and $n_{f,x}$. Moreover, we see that for any horizontal array M_s for the interconnected case is higher, since, as explained above, for isolated strips M_s has the same value as for a single strip, $J_c a/2$, due to the fact that current lines must close inside each filament and that the $\pm J_c$ interface is a straight vertical line.

The second difference is that the χ_0 dependence on the strip separation is opposite: whereas for isolated strips decreasing d_x results in a larger χ_0, for interconnected strips χ_0 decreases with decreasing d_x. For interconnected strips, we can take into account that the array substantially shield the magnetic field in the spaces between strips. Then, the magnetic behavior cannot qualitatively differ from considering an overall. As presented in Sec. 7.2.1, χ_0 monotonically increase with decreasing the thickness-to-width aspect ratio, so that arrays with higher d_x present higher χ_0 values. The effect of varying d_x for the isolated case is discussed above.

Another feature observed in the interconnected case is the presence of a kink (change in the slope) in the magnetization curve, particularly for the cases of large separation between strips. This effect is explained as follows. Since the magnetic moment is proportional to the area enclosed by the loops, current in the external strips contribute more to the magnetization than that in the inner ones. So, when the external strips become saturated, new current can only be induced in the central strip, having a lower contribution to the magnetization M, so that the M rate when H_a is increased is lower in magnitude. A similar effect has been predicted for rings in the critical-state model [140].

7.4.3 χ'' calculations

In this section we study the imaginary part of the ac susceptibility calculated from the magnetization loops obtained in section 7.4.2, which can be easily related to the ac loss by means of Eq. (6.9) [29]. Again, in this thesis we do not present the results for χ'; some calculations for horizontal arrays can be found in [144].

Dependence on strip separation

In Fig. 7.12 we present calculated results for χ'' as function of H_m for the same horizontal arrays discussed in the previous sections (with $b/a = 0.1$ and different separation distances d_x/a =2, 0.2, and 0.02). The two different cases of interconnected and isolated strips are plotted together for comparison.

As expected, all the calculated $\chi''(H_m)$ curves present a peak (and therefore a change of slope of the ac loss). This peak, however, is wider for the case of isolated strips, specially on the left part. This effect has been experimentally found in several works [145, 146, 147, 148, 149]. Actually, the cause of the disagreement between theoretical

predictions and experiments in these works is that they used models for single strips or disks, which yielded more narrow peaks. This peak widening can be explained by the critical-state model calculations presented in this chapter in the following way. The effect appears since the $M_i(H_a)$ curve becomes nonlinear at small applied field values because of the penetration of magnetic flux not only in the outer surface regions of the strips but also in the channels between strips, where the field magnitude is higher. This deviation from linearity in the $M_i(H_a)$ curve results in an increase of χ''.

Another interesting issue is the peak value of the ac susceptibility normalized to χ_0, χ''_{pk}/χ_0. The obtained results are $\chi''_{pk}/\chi_0 = 0.21$, 0.17 and 0.13 for $d_x/a = 2$, 0.2 and 0.02, respectively, so that a significant reduction of 41% for $d_x/a = 0.02$ is found. Notice that the reduction in χ''_{pk}/χ_0 when decreasing d_x/a is due to an increase of χ_0 rather than a decrease in χ''_{pk}. This lower-than-usual value in χ''_{pk}/χ_0 due to tape geometry has been experimentally found [146, 147].

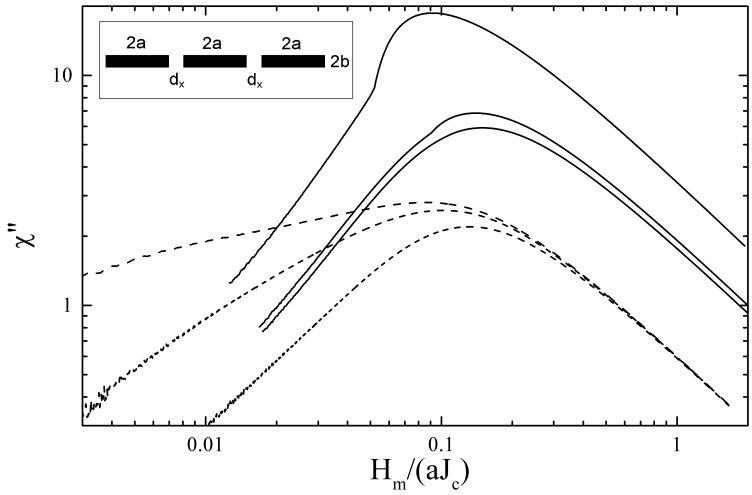

Figure 7.12: Imaginary ac susceptibility χ'' as a function of the ac applied field amplitude H_m corresponding to the $M_i(H_a)$ curves showed in Fig. 7.11 for horizontal arrays. The strips dimensions are $b/a = 0.1$. Solid lines are for the case of interconnected strips for d_x/a =2, 0.2, and 0.02 from top to bottom, while dashed lines are for isolated strips with d_x/a =0.02, 0.2, and 2 from top to bottom.

We also find that for interconnected strips χ''_{pk} increases with d_x, while it decreases for the isolated-strips case. Moreover, the χ''_{pk} dependence on d_x is only slight for the case of isolated strips but much more evident for the interconnected ones. These results can be understood from the magnetization curves of Fig. 7.11, in which we observe two important properties: χ_0 for interconnected strips increases with increasing d_x, while it decreases for isolated strips, and, most important, for interconnected strips, M_s has very different values for the different separations, while it remains constant for isolated strips, Sec. 7.4.2. Another characteristics observed in the two upper curves of Fig. 7.12 is a kink at a particular field value, that is directly related to the presence of a similar

kink in the magnetization data shown in Fig. 7.11. This kink was already predicted for rings [140] and later experimentally observed [150]. Furthermore, experimental evidence of a kink in actual superconducting tapes was shown for the case of a Ag/Bi-2223 tape with the superconducting core shaped as a circular shell [151] or two concentric elliptical shells [124].

As expected, the high-H_m limit is proportional to H_m^{-1}. However, although for isolated strips curves it is independent on d_x, for interconnected ones it is shifted upwards with increasing d_x. This is so because χ'' for high H_m is proportional to M_s, which for interconnected strips increases linearly with increasing d_x, (Sec. 7.3.2), while M_s for isolated strips do not depend on strip separation.

Dependence on the number of strips

In Fig. 7.13 we present the calculated results for horizontal arrays with $b/a = 0.01$, $d_x/a = 0.02$ and several number of strips, $n_{f,x} = 1, 2, 3, 5$ and 9. We consider the isolated strips case only, in order to compare our results with the analytical prediction for an infinite array of thin strips, done by Mawatari [92]. In Fig. 7.13 we also plot the calculated results for a single strip with $b/a = 0.01$ as well as the corresponding curve calculated from the thin strip limit analytical formulae of Eq. (7.2.1) [87]. On the other limit, we check that the results for a large number of strips tend to the analytical results for an infinite array of thin strips [92], although 9 is not a sufficient number for approaching the limiting case (higher number of strips yield values closer to infinite array results; not shown for clarity). The general trend observed with varying $n_{f,x}$ is that χ'' increase with $n_{f,x}$, which is due to the increase of the number of flux channels, enhancing the flux compression effects [68, 69, 121].

7.5 Matrix arrays and interleaved geometry

An important result of this work is that the general trends of the magnetic behavior of a matrix result from the composition of the properties of both the vertical and horizontal array that forms it. This the reason why we studied first the vertical and horizontal arrays in detail. We now study the matrix geometry taking into account the previous results.

7.5.1 Current profiles and magnetic flux lines for matrices

In Fig. 7.14 we show the calculated current penetration profiles and magnetic flux lines for a 3×3 matrix array of strips with $b/a = 0.1$ under an applied field of $0.2H_p$ for Fig. 7.14(a,b,c) and $H_a = 0.1H_p$ for 7.14(d,e). In this figure the three upper profiles correspond to the interconnected case, while the two bottom ones are for isolated strips.

For interconnected strips the general trend of shielding the region bounded by the superconductor, including gaps between strips, is clearly seen. An interesting feature is that a very satisfactory magnetic shielding is achieved for the three different matrices.

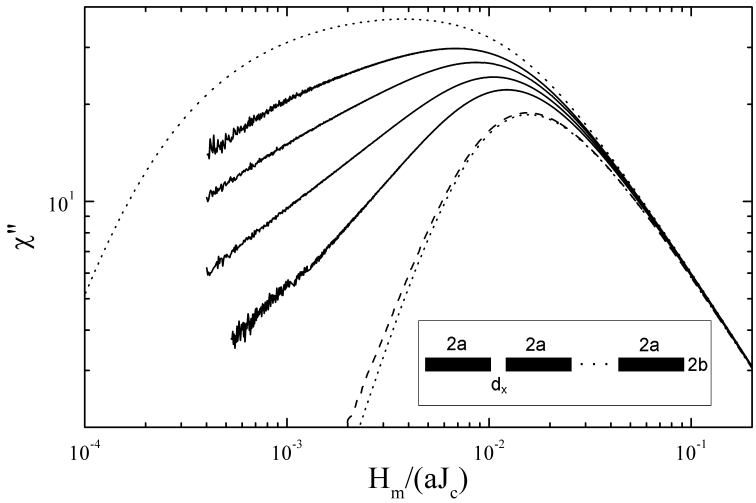

Figure 7.13: Imaginary ac susceptibility χ'' as a function of H_m for horizontal arrays with several number of strips $n_{f,x}$ (solid lines), corresponding to $n_{f,x} = 9, 5, 3, 2$ from top to bottom, compared to a single strip (dashed line) and the 1D analytical limits for a single thin strip calculated from Eq. (7.2.1) (lower dotted line) and an infinite horizontal array of thin strips [92, 130] (upper dotted line). The strip aspect ratio is $b/a = 0.01$ and their separation is $d_x/a = 0.02$.

However, this shielding is, for the values of the applied field considered here, basically produced by the strips in the two outer vertical columns, which are largely penetrated by currents. Only a small current density penetration is needed in the upper and bottom strips of the inner column to create a fine adjustment of the field in the central region.

In Figs. 7.14(d,e), corresponding to isolated strips, the effect of flux compression along the vertical channels, that include the gaps and the surrounding regions, is clearly seen in the case of the smallest separation distance. Moreover, the magnetic field is shielded in the vertical gaps between rows but it is enhanced in the horizontal gaps between columns. Then, for isolated strips, magnetic interaction between rows and columns have opposite effects.

7.5.2 χ'' calculations for matrices

In this section we do not show the magnetization curves for the sake of brevity; some calculated $M_i(H_a)$ curves can be found in [71]. Some calculations for χ' as a function of H_m can be found in [70][1].

The calculated results for χ'' are presented in Fig. 7.15 for $b/a = 0.1$ and several strip separations. In order to study the effect of varying the vertical separation, in Fig.

[1]In caption of Fig. (2) of [70] there are several typographical errors. The figure is for $h/a = 0.2$ (our d_y/a) and $d/a = 2, 0.2, 0.02, 0$ (our d_x/a) from top to bottom for interconnected strips and $d/a = 0.02, 0.2, 2, \infty$ for isolated strips. The appendix in that paper should not be published and must be ignored.

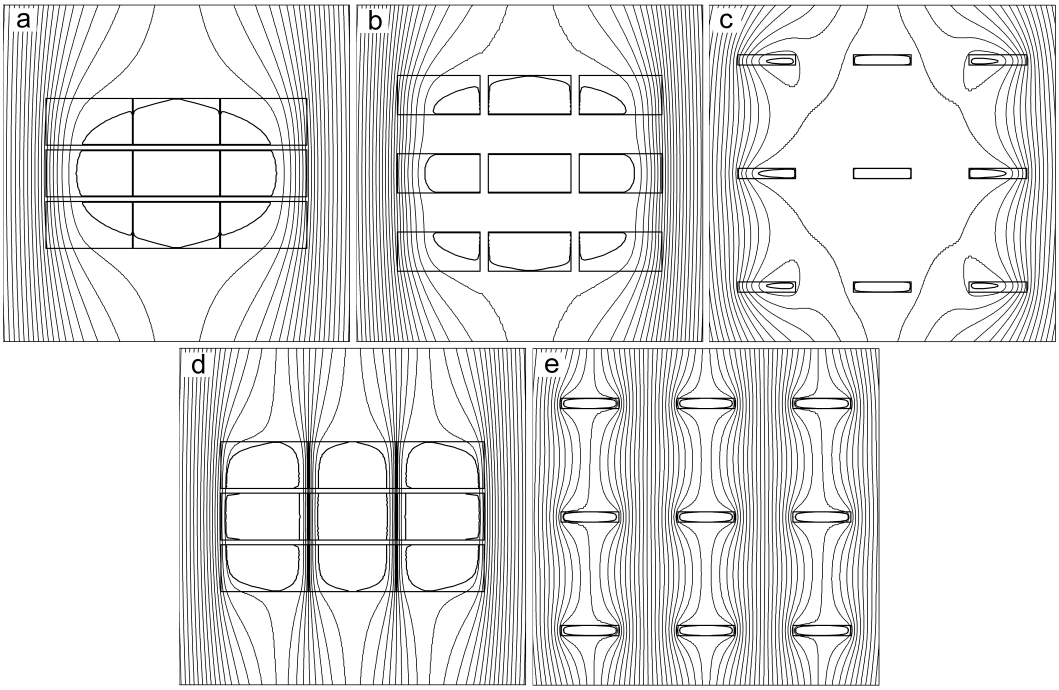

Figure 7.14: Current profiles (thick lines) and magnetic flux lines for a 3×3 matrix array of strips with $b/a = 0.1$ and $d_x = d_y = 0.02a$ (a,d), $d_x = d_y = 0.2a$ (b) and $d_x = d_y = 2a$ (c,e). Upper graphs (a,b,c) are for interconnected strips immersed in an applied field $H_a = 0.2H_p$, while bottom ones (d,e) are for isolated strips with $H_a = 0.1H_p$. The vertical scale has been expanded for clarity.

7.15(a) we present the $\chi''(H_m)$ curves for $d_x/a = 0.2$ and $d_y/a = 0, 0.02, 0.2, 2, \infty$, while in Fig. 7.15(b) we present results for $d_y/a = 0.2$ and $d_x = 0.02, 0.2, 2, \infty$ to study the d_x dependence.

As expected, the effect of varying d_y is the same as for vertical stacks, that is, χ'' decrease with decreasing d_y/a for both isolated and interconnected strips and the peak shifts to higher values (Sec. 7.3.3). Moreover, the high H_m limit, where $\chi'' \propto H_m^{-1}$, independent of d_y but the curve is higher for interconnected strips. This is so because for the high-H_m limit χ'' is proportional to the saturation magnetization [see Eq. (7.9) and discussion below][29], which for the interconnected case is higher than for the isolated one, Sec. 7.4.2.

With varying d_x, the $\chi''(H_m)$ curve changes in the same way as for horizontal arrays (Sec. 7.4.3), so that both a peak widening for isolated strips and a kink in interconnected ones appear. Also, there appears the same dependence of the height and position of the peak on d_x, that is, for interconnected strips the peak is higher and shifts to lower H_m with increasing d_x, while for isolated strips is the opposite.

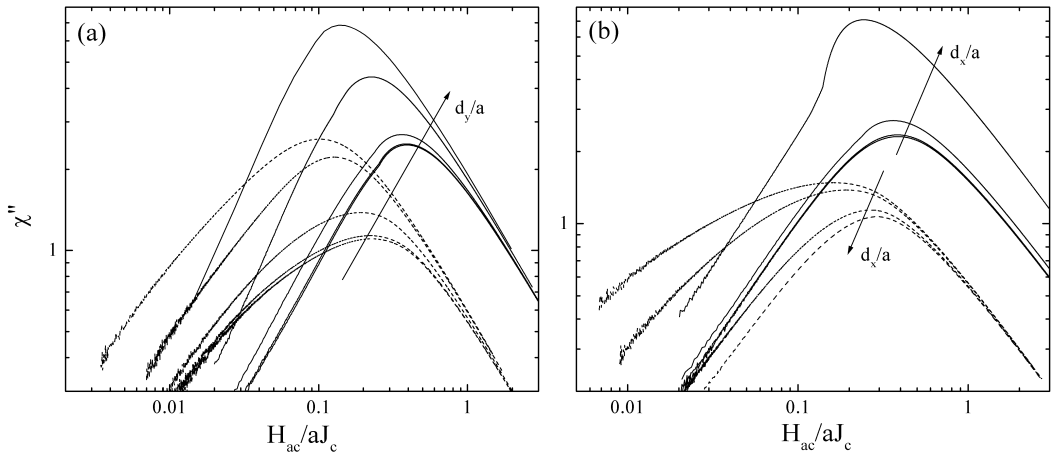

Figure 7.15: Imaginary part of the ac susceptibility χ'' as a function of H_m/aJ_c for 3×3 matrix arrays of strips with $b/a = 0.1$. Solid lines are for the interconnected strips case, while dashed ones are for isolated strips. Figure (a) is for $d_x/a = 0.2$ and $d_y/a = 0, 0.02, 0.2, 2, \infty$ in the arrow direction. Figure (b) is for $d_y/a = 0.2$ and $d_x/a = 0, 0.02, 0.2, 2$ for interconnected strips and $d_x/a = 0.02, 0.2, 2, \infty$ for isolated ones in the arrow direction.

7.5.3 Comparison with interleaved geometry

We next present a comparison between matrix arrays and the interleaved geometry, which is commonly found in Ag/Bi-2223 tapes. Here we only consider the more interesting case of isolated strips, although the results for the interconnected one can be found in [139].

In Fig. 7.16 we show the calculated field lines and current profiles for a 5×3 matrix array of strips (a) and a 16-strip interleaved geometry (b) with $b/a = 0.1$ corresponding to an applied field $H_a = 0.2H_{p,1}$, where $H_{p,1}$ is the penetration field of one of the strips of Eq. (7.5). In Fig. 7.17 we show the calculated χ'' as a function of $H_m/(aJ_c)$.

The first important result is that χ'' (and also the ac loss) is larger in general for interleaved arrays than for matrix ones. This effect is explained as follows. In a regular matrix array the strips are stacked in columns, so that the strip in the central row of each column is shielded by the top and bottom ones, reducing the overall ac loss. This shielding is not present in the interleaved geometry. Thus, the described effect creates a large difference between interleaved and matrix geometries, in both the magnitude of the loss and the peak position. Another interesting issue is that χ'' is larger for the case of interleaved strips than for a single strip, which means that the bending and focusing of the magnetic field between the strips create an effective field around them larger than the applied field. As expected, the high-H_m limit coincide for all cases, since M_s is the same (Sec. 7.4.3).

The main results of the model are in agreement with some recently published experimental data. Both Suenaga [148] and Leghissa et al [152] found that Bi-2223 tapes

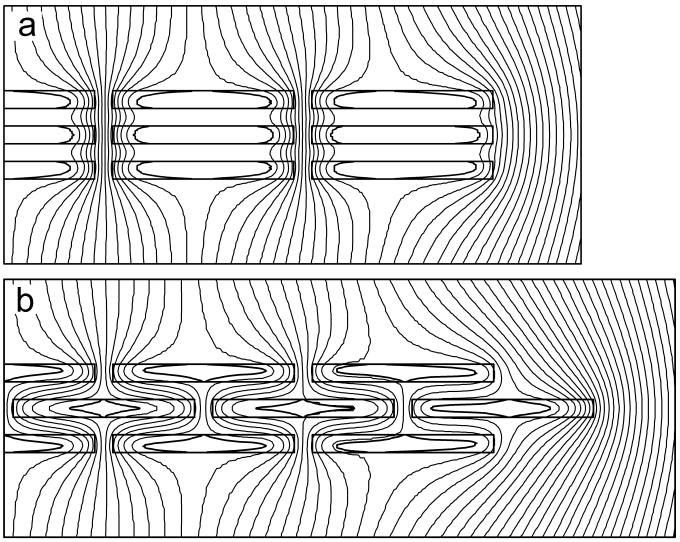

Figure 7.16: Magnetic field lines and current profiles for a 5×3 matrix array of strips (a) and a 16-strips tape in interleaved arrangement (b) with $a/b = 0.1$ and vertical and horizontal separations $d_y/a = 0.2$ and $d_x/a = 0.2$, respectively. Both figures correspond to the isolated case. The applied field is $0.2H_{\mathrm{pen},1}$, where $H_{\mathrm{pen},1}$ is the penetration field of one of the strips. The vector potential difference between flux lines for both figures is the same.

arranged in interleaved geometry have larger magnetic ac loss than that corresponding to matrix filament arrangements, except for low values of the applied magnetic field. This is the behavior observed in Fig. 7.17.

7.6 Elliptical cross-section

The MEM procedure presented in chapter 6 can be also applied to infinitely long superconducting strips with an elliptical cross-section. In [32, 33] we numerically calculated the current profiles and the height and position of the maximum in the $\chi''(H_m)$ curve, χ''_{pk} and $H_{m,\mathrm{pk}}$, respectively. The calcultations for $H_{m,\mathrm{pk}}$ can be used by experimentalists to extract J_c from measured $\chi''(H_m)$ curves. For this reason, in [33] we presented a table for $H_{m,\mathrm{pk}}$ and χ''_{pk} for several values of b/a, as well as an analytical fit of $H_{m,\mathrm{pk}}$ for $b/a < 1$.

Taking into account the numerically calculated profiles, in [32] we also presented an approximate analytical model assuming current profiles with elliptical shape. This model, although simple, satisfactorily reproduces the results for the $\chi''(H_m)$ curves obtained by the MEM calculations. Exact analytical expressions for H_p and M_s can also be found in that paper.

In [32, 33] we compare experimental data of the $\chi''(H_m)$ curve for a monofilamentary elliptical tape with the corresponding theoretical results, showing a good agreement.

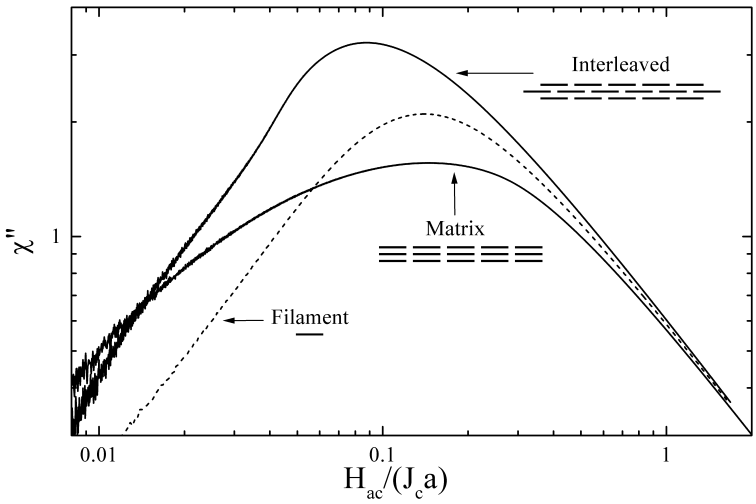

Figure 7.17: Imaginary part of the ac susceptibility χ'' as a function of H_m. Solid lines are for the matrix and interleaved multifilamentary tapes of Fig. 7.16, while the dashed line is for a single strip with the same aspect ratio as those in the arrays ($b/a = 0.1$).

7.7 Chapter summary and conclusions

In this chapter we thoroughly study the real χ' and imaginary χ'' ac susceptibilities in a rectangular strip; tables with calculated data are presented in [85]. After this, we calculate and discuss the magnetic properties, such as current profiles, magnetic flux lines, magnetization and χ'', for arrangements of strips in vertical stacks, horizontal arrays, matrices and interleaved geometry [71, 70, 144]. For the latter three arrangements we consider both the cases of isolated and interconnected strips, presenting a very different behavior.

The most interesting issues for rectangular strips are that the low-H_m limit for χ'' and $1 + \chi'$ is proportional to H_m for any a/b, while it is lower and proportional to H_m^2 for the analytical formulae derived from 1D models for thin strips. This difference is due to the assumption of uniform current density across the thickness for the 1D analytical models. Another interesting feature is that the peak in the $\chi''/\chi_0(H_m)$ curve presents a minimum at $a/b = 0.5$, being 18% and 15% lower than for infinite slabs and thin films, respectively. The high-H_m limits for the $\chi''(H_m)$ and $\chi'(H_m)$ curves are proportional to H_m^{-1} and to $H_m^{-3/2}$, respectively, as for longitudinal applied fields [29].

For vertical stacks of $n_{f,y}$ strips we find that both χ_0 and χ'' monotonically decrease with decreasing d_y/a. The high-d_y/a limit for χ'' corresponds to that for one of the strips taken independently, while the low-d_y/a limit approaches the value of χ'' for a thicker strip with aspect ratio $n_{f,y}b/a$, rather than a single tape with the overall shape including the gaps. For a fixed separation and b/a, χ'' decreases with increasing the number of strips. We also found that the qualitative behavior of vertical stacks depends on d_y/a but not d_y/b.

The study of horizontal arrays revealed that the interconnected and isolated strips cases are very different qualitatively. The magnetic properties for the interconnected case with low separation are very similar to those of a sample with the overall shape, but not for the isolated case. For the latter, there appears flux compression in gaps between strips, from which current density penetrates deeper. This is the origin of a widening of the peak in the $\chi''(H_m)$ curve as compared to single strips or vertical stacks. The ratio χ''/χ_0 for the calculated cases of isolated strips can be up to 41% lower for the lowest calculated d_x/a. This reduction is due to an increase in χ_0 rather than a decrease in χ''. The d_x dependence of χ_0 and χ'' is opposite for isolated and interconnected cases; they decrease with increasing d_x/a for isolated strips, while they increase for interconnected ones. With increasing the number of strips, both χ_0 and χ'' increase for both isolated and interconnected cases and $\chi''_{\rm pk}/\chi_0$ decreases for isolated strips.

The magnetic behavior of matrix arrays is a composition of that for vertical and horizontal arrays. As a consequence, the effect in χ'' of varying d_x and d_y is the same as those for horizontal and vertical stacks, respectively. Considering interleaved arrangements, its magnetic behavior for the isolated case is very different from matrix arrays. Flux lines for the interleaved geometry wrap around strips and flux compression is much smaller than in matrix arrays. As a result, the $\chi''(H_m)$ curve for interleaved arrangements does not present the characteristic peak widening for matrix arrays. The peak in χ'' for matrices is lower due to the magnetic shielding from vertical stacking, which do not appear for interleaved arrangements.

CHAPTER 8

Superconducting tapes with ac transport current

The study of the transport ac loss in superconducting tapes and wires is not only useful to reduce the energy dissipation but also to characterize some superconducting material properties [153, 41]. Actual superconducting tapes and wires consist of superconducting filaments embedded in a conducting matrix and covered by a conducting sheath (see introduction in chapter 7). The study of multifilamentary cross-sections with transport current is not only useful for actual composite conductors in self-field but also for magnetically interacting tapes or wires [108, 154, 155, 156, 157, 158].

In this chapter we systematically study current profiles and ac loss for a single rectangular strip with finite thickness and a set of strips arranged linearly or in matrix configuration to simulate actual superconducting tapes [159, 160, 161]. We consider the case that the rectangular strips are connected in parallel to an ideal alternating current source with amplitude I_m. This connection in parallel is found in real superconducting tapes with no twisting nor resistive barriers thanks to the metallic matrix or substrate. However, we assume that the contribution of the metallic region to the loss is negligible in front of the hysteretic loss of the superconductor. This assumption is usually valid for low enough frequencies [162].

8.1 Previous existing results

The critical-state model with constant critical-current density J_c (Sec. 2.3.3) [7, 9] has been shown to be a useful tool to describe the ac loss of actual superconducting wires. It was first applied to analytically calculate the transport ac loss for simple geometries, such as a cylinder [9], a circular tube or an infinite slab [163]. Some years later, Norris extended the application of London's formula for cylinders [9] to a bar with elliptic cross-section with an arbitrary value of semiaxis (aspect) ratio, derived analytically the loss Q_t

for an infinitely thin rectangular strip, and calculated Q_t analytically for a rectangular bar with arbitrary width-to-thickness aspect ratio at $I_m/I_c = 1$ [86]. His formulae for elliptic bar and thin strip are, respectively,

$$\frac{2\pi Q_t}{\mu_0 I_c^2} = (2-i)i + 2(1-i)\ln(1-i) \approx i^3/3, \tag{8.1}$$

$$\frac{2\pi Q_t}{\mu_0 I_c^2} = 2[(1+i)\ln(1+i) + (1-i)\ln(1-i) - i^2] \approx i^4/3, \tag{8.2}$$

where $i = I_m/I_c$ and the approximation is made for low i. Further theoretical advances and the discovery of HTS materials motivated the analytical study of other interesting geometries, such as a cylinder with two concentric circular shells with different J_c [48] and some multifilamentary geometries, like vertical and horizontal arrays of an infinite number of thin strips [164] or double thin strips [131].

Apart from the mentioned analytical studies, some numerical models within the critical-state model have been developed to describe superconductors with transport current. Norris presented the first numerical calculations for a square bar [165] in the early seventies. More recently, the geometry of rectangular strips with arbitrary thickness was studied by Fukunaga *et al* [79], Däumling [80] and ourselves [84], after which extensive work on multifilamentary tapes was done by Fukunaga *et al* [166, 159]. An alternative approach from the critical-state model is to assume a certain $E(J)$ dependence as $E(J) = E_c(J/J_c)^n$, where E is the electrical field. An interesting model considering this assumption is that developed by Brandt [88] for superconducting strips in magnetic applied fields, which was extended for the transport current case by Rhyner [167] and Yazawa *et al* [168]. Same as our approach, this model requires numerical calculations inside the superconductor only. Other authors applied conventional finite-elements techniques to the transport case in multifilamentary tapes, such as Stavrev *et al* [133, 169].

8.2 Single rectangular strip

We consider first a superconducting rectangular strip with dimensions $2a \times 2b$ and constant J_c carrying an ac transport current with amplitude I_m. The results and discussions presented in this section can be found in [84].

8.2.1 Analytical calculation of ac loss at $I_m = I_c$

When the amplitude of the ac current satisfies $I_m = I_c$, the rectangular strip is fully penetrated by uniform current density at peak current. Taking into account that for a rectangular strip the kernel corresponds to the geometrical center, the normalized ac loss $q_t \equiv 2\pi Q_t/(\mu_0 I_c^2)$ can be derived by using Eqs. (6.14) and (6.2), obtaining [84, 170]

$$\begin{aligned} q_t(I_m/I_c) &= \frac{2\pi Q_t}{\mu_0 I_c^2} = 4\ln 2 - \frac{7}{3} \\ &- \frac{1}{3}\left[\frac{b^2}{a^2}\ln\left(1+\frac{a^2}{b^2}\right) + \frac{a^2}{b^2}\ln\left(1+\frac{b^2}{a^2}\right)\right] \end{aligned}$$

$$+ \quad \frac{2}{3}\left[\frac{b}{a}\arctan\frac{a}{b}+\frac{a}{b}\arctan\frac{b}{a}\right]. \tag{8.3}$$

The normalized ac loss versus a/b at $i = 1$ calculated from Eq. (8.3) is shown in Fig. 8.1. With increasing a/b from 1 to ∞, q_t decreases monotonically from 1.0244 to 0.7726. We should mention that the above analytical calculation for $i = 1$ has followed exactly Norris' procedure but improved greatly his numerical evaluation made in [86, 165].

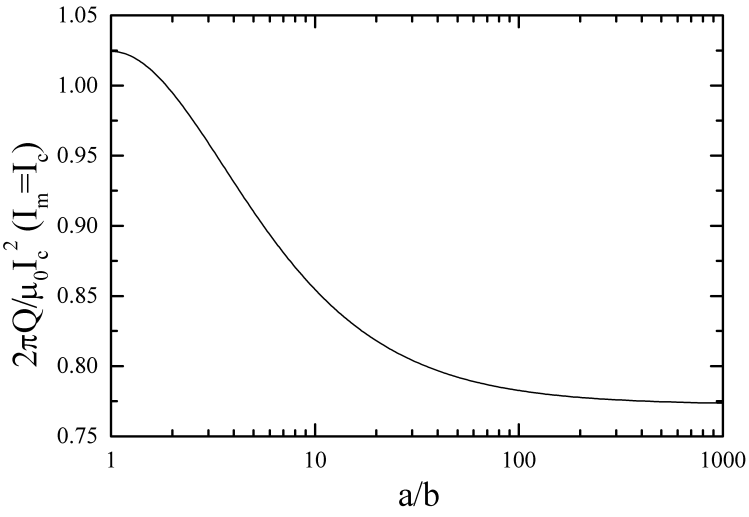

Figure 8.1: Analytically calculated $2\pi Q/\mu_0 I_c^2$ for a rectangular superconducting bar at $i = 1$ as a function of a/b.

8.2.2 Numerical results and discussion

For arbitrary values of I_m/I_c numerical calculations are needed. For this purpose we use the MEM procedure, presented in Sec. 6.2. We divide the rectangular bar into $2n_x \times 2n_y \approx 4 \cdot 10^4$ elements, being n_x and n_y the divisions in the a and b directions, respectively. To achieve an optimum accuracy, we choose n_x and n_y so that $n_x/n_y \approx \sqrt{a/b}$ and we consider the use of $m_m = 5$ to 40 current steps, increasing with increasing a/b and decreasing i.

In order to show the correctness of the calculated front, we plot in Figs. 8.2(a) and 8.2(b) for $a/b = 100$ the computed strip current density along the broad width at $i = 0.1$, 0.2, 0.4, and 0.6 using $m_m = 1$ (a) and 2 (b), which is compared with the Norris' analytical result of thin strip [86]. We see that the latter is quite a good average of the former, and dividing the elementary J_c into five equal steps improves the coincidence between both. We note that for our numerical calculations with $m_m > 1$ we obtain a current-free and flux-free zone, a zone with $J_z = J_c$ and a layer of only one-element thickness with $J_z < J_c$ in between, which appears to better approach the smoothly curved front corresponding to the exact solution [84]. Then, the results in Fig. 8.2

not only justify the correctness of the calculated results, but also show that in the 1D calculation for a thin strip, the nonzero strip current density covering a large portion of the strip is actually an integrated effect between $y = \pm b$ for the actual $J(x, y)$ that follows basically the same rules of the original Bean model.

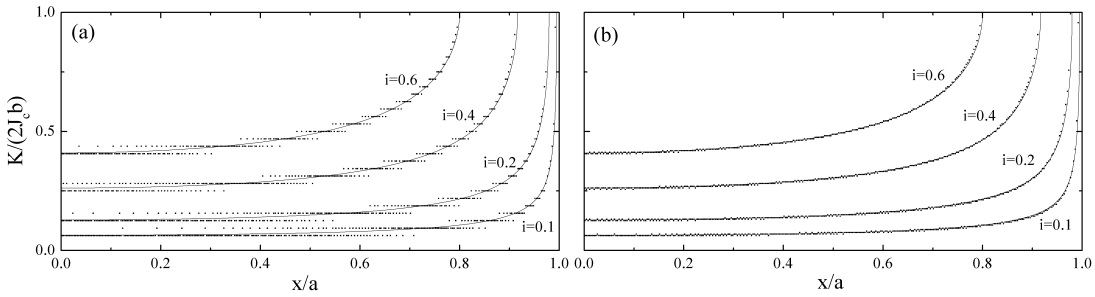

Figure 8.2: Strip current density K (current density integrated between $y = \pm b$) for $a/b = 100$ at $i = 0.1$, 0.2, 0.4, and 0.6 calculated numerically with single-step (a, squares) and five-step (b, square) elementary current filling procedures compared with Norris' [86] analytical result of thin strip (solid lines).

In Fig. (8.3) we present the numerical results for the ac loss as a function of i for $a/b = 1$, 3, 10, 30, 100 and 300. Since for the transport case all electromagnetic properties are independent on the strip orientation, results for $a/b < 1$ are the same as those for $b/a > 1$. As a consequence of the discretization into elements, the $q_t(i)$ curve present some oscillations with varying i for high a/b and low i. Then, the line thickness in Fig. 8.3 can be considered as the numerical calculation error, having a magnitude of a few percent. In order to help the comparison between our calculations and experimental results, in [84] we present a table with some numerical results and an approximate formulae for $q_t(i, a/b)$ with a maximum departure from the calculations of a 4%.

From the results in Fig. 8.3 several features may be observed. The normalized ac loss at any given value of i decreases monotonically with increasing a/b from 1 to ∞. The $q_t(i)$ curve for $a/b = 1$ is only slightly above that of the Norris ellipse; the difference ranges from 29% to 2.4% for $i = 0.1$ to 1. A better overall agreement between both is found when $a/b = 3$. A rough i^3 dependence occurs for $1 \leq a/b \leq 100$, although it may occur at lower i when a/b is larger.

Norris has attributed the difference between the i^3 and i^4 dependence of elliptical bars and thin strips to the neglect of current penetration from the broad sides in the latter case [86]. Considering a rectangular strip, he has estimated that the thin-strip approximation in not valid when $i < \pi b/a$ [86]. From our calculation, we see that Norris' statement is qualitatively correct. However, a practically important discovery of our calculation is that for rectangular bars, the i^4 behavior at $i \sim 0.1$ can roughly occur only when $a/b > 3 \times 10^3$, which can be realized by the tendency of the calculated a/b dependence. This condition is two orders of magnitude stricter than Norris' estimation, which has

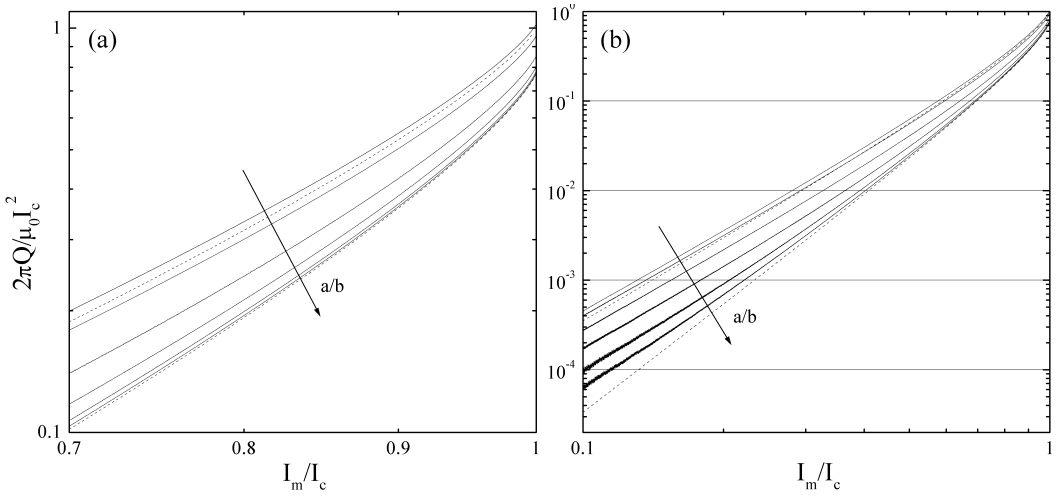

Figure 8.3: Numerically calculated $2\pi Q/\mu_0 I_c^2$ as a function of I_m/I_c from 0.7 to 1 (a) and from 0.1 to 1 (b) for a rectangular bar with constant critical-current density at transverse aspect ratio $a/b = 1, 3, 10, 30, 100$, and 300. The arrows show the increase in a/b. Results for the Norris ellipse and strip, Eqs. (8.1) and (8.2) , are included for comparison (upper and down dashed lines).

been used for the discussion of experimental data [41]. Our accurate results show that if J_c is constant, the information that can be obtained from ac loss measurements of Bi-2223/Ag tapes (typically with $a/b \sim 15$) is their overall cross-sectional shape and the value of a/b. Equation (8.1) should be valid if the overall shape is close to an ellipse; if the superconducting core has uniform thickness in the major portion of its cross-section, Q_t should decrease with increasing the aspect ratio, as it is the case of rectangular strips, even if the edges of the tape are curved.

8.3 Horizontal arrays

Once the ac loss for a single strip is calculated and discussed, in Secs. 8.3 and 8.4 we study the interaction between several strips of dimensions $2a \times 2b$ arranged linearly with constant spacing. For the transport case, the electromagnetic properties of the array are independent on its orientation, different from the magnetic case, for which the applied field provides a privileged direction. Then, a horizontal array of filaments with dimensions a and b has exactly the same properties as a vertical one with filaments with dimensions b and a. For clarity of exposition, in this chapter we consider filaments with $a/b \geq 1$ and we refer to horizontal arrays or vertical stacks as linear arrangements of strips aligned in the a or b directions, respectively. As is explained below, the results for horizontal arrays and vertical stacks present some qualitative differences.

In this section we study the current profiles, magnetic field lines and ac loss for horizontal arrays of $n_{f,x}$ strips separated a distance d_x. All the results and discussions

in sections 8.3, 8.4 and 8.5 can also be found in [94].

8.3.1 Dependence on horizontal separation

Current profiles and magnetic flux lines

To illustrate the current penetration process in a horizontal array, we calculate the current profiles corresponding to $i \equiv I_m/I_c = 0.1, 0.2, 0.4, 0.6$ and 0.8 for a three-strip horizontal array with $a/b = 20$ and $d_x/a = 0.02$, 0.2 and 4 (Figs. 8.4(a,b,c) respectively). The arrays are artificially drawn with the same separation to facilitate the profiles comparison. As can be seen in the figure, current penetrates from the superconductor borders and vertices to inside, being the penetration deeper from the external vertical border of the external strips, so that the current carried by the external strips is higher. The current profiles for low d_x/a, Figs. 8.4(a,b), do not differ significantly from those for taking the array as a single strip with the overall dimensions, except near the strip gaps for $d_x/a = 0.2$, Fig. 8.4(b). When the distance between strips increases (Fig. 8.4(c)), the current penetration from the inner boundaries is enhanced and the field-free core in the outer strips moves towards the strip center. Moreover, the current fraction carried by each strip in the array becomes more similar to each other with increasing d_x/a. Then, the current profiles for the large d_x/a limit would be identical for all the strips and equal to those for each of the superconducting strips taken independently.

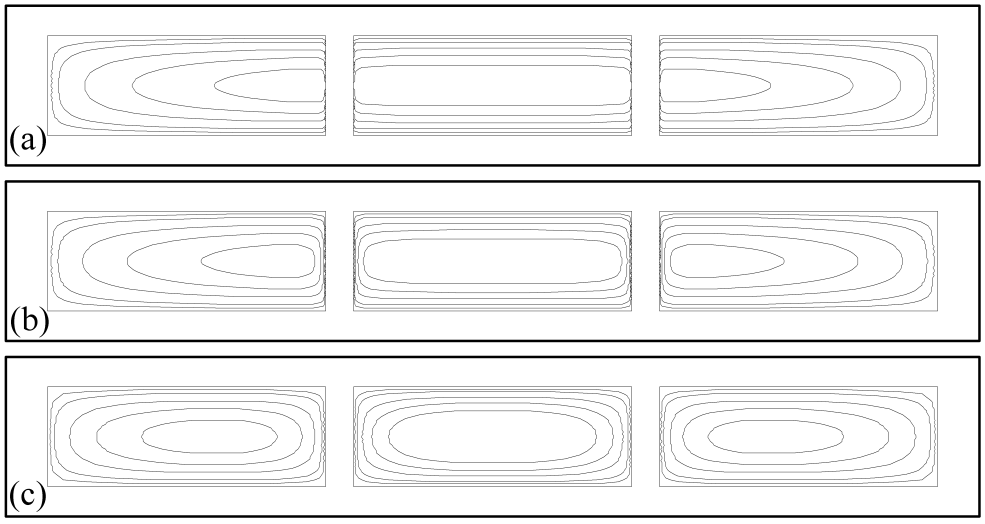

Figure 8.4: Current fronts for horizontal arrays made of three strips with aspect ratio $a/b = 20$ and several horizontal separations $d_x/a = 0.02$, 0.2 and 4 (a,b,c). The current fronts correspond to $i = I_m/I_c = 0.1$, 0.2, 0.4, 0.6 and 0.8 from outwards to inwards. Vertical axis has been expanded and strip separations have been drawn as the same for visualization.

We notice that the high d_x/a limit is reached much slowly for the transport case than for the magnetic one, that is, for arrays of strips under a uniform applied ac

field (compare Figs. 7.10 and 8.4) [71, 144]. This is because the magnetic induction magnitude generated by one of the strips $B_{\rm str}$ is roughly proportional to $1/r$ for the transport case, whereas for the magnetic case the net current in a strip is zero, so that the dipolar contribution is the most important one and $B_{\rm str} \propto 1/r^2$.

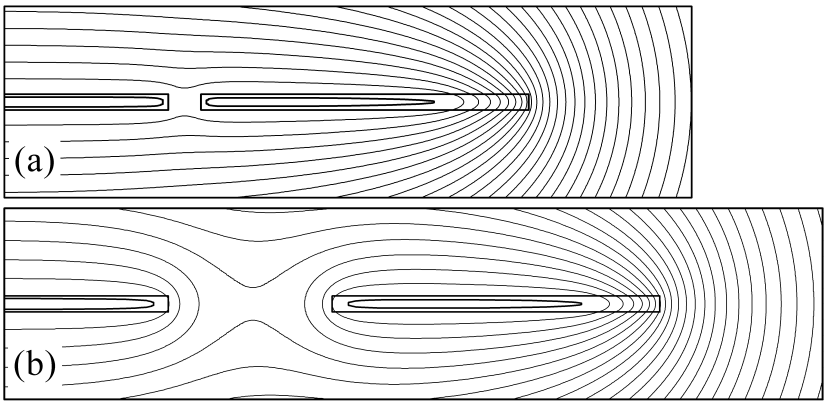

Figure 8.5: Current fronts (thick lines) and magnetic flux lines (calculated as $A_{z,c} - A_z(\mathbf{r})$ level curves) for horizontal arrays made of three strips with aspect ratio $a/b = 20$ and separation $d_x/a = 0.2$ (a) and $d_x/a = 1$ (b) carrying a transport current $I = 0.6 I_c$. Only the right half part of the tape is plotted. The $A_{z,c} - A_z(\mathbf{r})$ variation between level curves is the same for both plots.

In Fig. 8.5 we plot the vector potential difference $A_{z,c} - A_z(\mathbf{r})$ level curves and the current profile for a three-strip array with $a/b = 20$ and $d_x/a = 0.2$ (Fig. 8.5(a)) and $d_x/a = 1$ (Fig. 8.5(b)) carrying a current $i = 0.6$. The presented $A_{z,c} - A_z$ level curves can be either regarded as magnetic field lines (Sec. 6.1.3) [88, 71] or, in the region where $J_z = J_c$, as the ac loss density level curves. This latter property of $A_{z,c} - A_z$ can be deduced from Eq. (6.14) considering that the only region where $0 < J_z < J_c$ is a thin layer of one-element width surrounding the flux-free core, where $A_{z,c} - A_z = 0$. As expected from the current profiles in Fig. 8.4, if the separation d_x/a is low enough (Fig. 8.5(a)), the vector potential, the magnetic field and the current profile are very similar to those for a single strip with the overall dimensions. If d_x/a increases, figure 8.5(b), these electromagnetic quantities progressively change to approach those for one of the superconducting strips taken independently. Another important issue is that the magnetic field between the strips is significantly lower than in the outer region. Moreover, the magnetic flux between two filament field-free cores is checked to be zero.

Finally, as a check of our numerical calculations, in Fig. 8.6 we present the numerical results of the sheet current density K (current density integrated over the thickness) for a two-strip horizontal array with compared to the exact analytical solutions found by Ainbinder and Maksimova for a double thin strip [131]. The obtained sheet current corresponds to $a/b = 100$ and $d_x/a = 2$ and $d_x/a = 0.2$ for Figs. 8.6(a) and 8.6(b), respectively, and several normalized current values. As can be seen in the figure, the

analytical profiles clearly agree with the numerical ones.

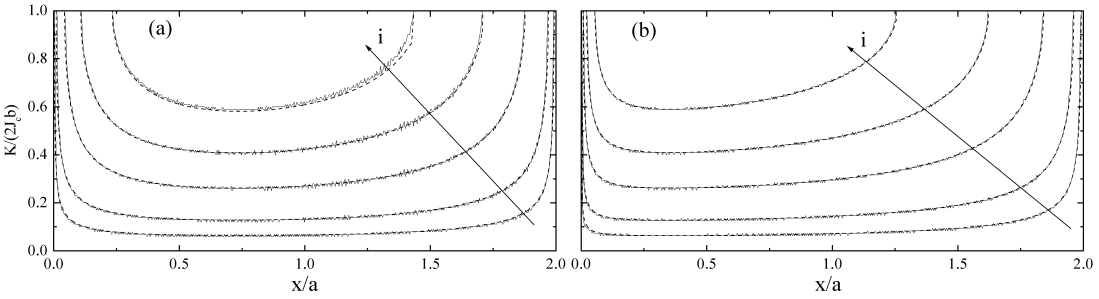

Figure 8.6: Sheet current density K profiles for a horizontal array of two strips with $a/b = 100$, $d_x/a = 2$(a) and $d_x/a = 0.2$(b), and $i = 0.1, 0.2, 0.4, 0.6$ and 0.8 in the arrow direction. Solid lines correspond to our numerical results, while dashed ones correspond to the analytical formulae in [131] for a double thin strip.

Normalized ac loss

The normalized ac loss $q_t = 2\pi Q_t/\mu_0 I_c^2$ as a function of the reduced current $i = I_m/I_c$ corresponding to a three-strip horizontal array with $a/b = 20$ and several d_x/a is plotted in Fig. 8.7. The curves for one isolated strip with $a/b = 20$ and the well-known cases of ellipses and thin strips, given by Eqs. (8.1) and (8.2), are also plotted for comparison. For all cases I_c is the total critical current for the specific geometry. The infinite separation case ($d_x/a = \infty$) for a set of $n_{f,x} = n$ aligned strips can be calculated from the curve for a single strip $q_t(i, n_{f,x} = 1)$ as $q_t(i, n_{f,x} = n) = q_t(i, n_{f,x} = 1)/n$, since for $d_x/a = \infty$ the strips do not interact to each other and $I_c(n_{f,x} = n) = nI_c(n_{f,x} = 1)$. This ac loss reduction due to magnetic decoupling of the filaments can also be obtained by covering the filaments with an ideally soft ferromagnetic material, that is a LHI material with high χ, [154].

As can be seen in Fig. 8.7, the curves for three strips present a sudden increase in the slope at a certain i value between 0.9 and 1, which corresponds to the point that the external strips are fully penetrated by current, $i_{\rm pe}$. This effect can be explained as follows. The vector potential difference, and so the ac loss density, increases in magnitude from the field-free core outwards (Fig. 8.5). Since for $i > i_{\rm pe}$ the only field-free zone belongs to the central filament, the ac loss density in the external strips increases more for the same current increment than if $i < i_{\rm pe}$. Consequently, this slope increase is higher for larger filament separation, which is consistent with Fig. 8.7. The presence of a kink has also been theoretically predicted for geometries with discontinuities of the J_c value in the cross-section [48, 171]. It is also interesting that the ac loss decreases when the horizontal separation increases for any i below 0.97. Furthermore, for $i \leq 0.97$ all calculated curves for nonzero d_x/a lay below Norris strip curve except for $d_x/a = 0.2$ which only presents lower loss between $i = 0.57$ and 0.97. The ac loss decrease with the

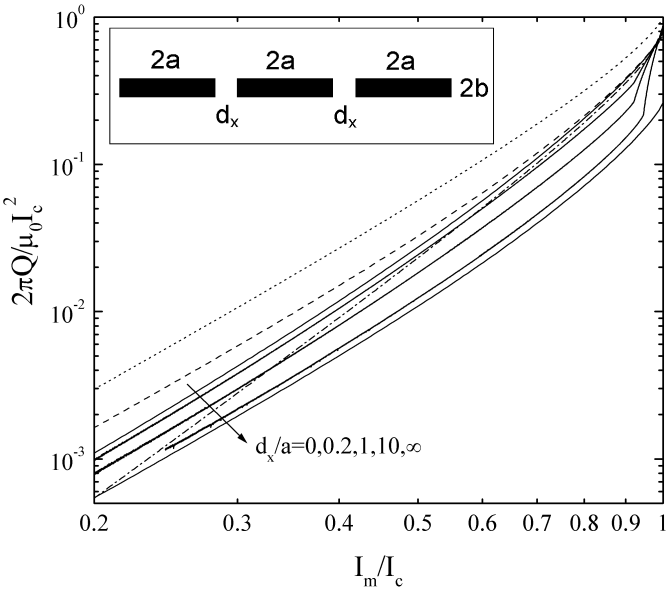

Figure 8.7: Normalized ac loss $2\pi Q_t/\mu_0 I_c^2$ as a function of the normalized ac field amplitude I_m/I_c. Solid lines correspond to horizontal arrays made of three strips with $a/b = 20$ and $d_x/a = 0, 0.2, 1, 10, \infty$ in the arrow direction, the dashed curve is for a rectangular strip with $a/b = 20$, dotted one is for the analytical formulae for ellipse in Eq. (8.1), and the dash-dotted curve is for a thin strip, Eq. (8.2).

strip separation for i below the kink is due to the decrease in the magnetic interaction with increasing the separation. This yields to a more similar current carried by each strip and a current profile more symmetric to each strip midplane (Fig. 8.4). Then, since the vector potential decreases with the distance to the field-free core, the average vector potential difference $A_{z,c} - A_z$ in each strip is lower, as can be seen in Fig. 8.5, where the $A_{z,c} - A_z$ level curves are plotted.

Another interesting issue is that the normalized ac loss for a horizontal array of strips with $a/b \geq 1$ and i below the kink is lower than that for one of the strips taken independently. This is because the normalized ac loss q_t for a strip monotonically decreases with increasing a/b [79, 80, 84], so that q_t for one of the strips is higher than the value for the horizontal array with $d_x/a = 0$ and, consequently, higher for any d_x/a.

All the features discussed in this section are general for any $a/b \geq 1$ ratio, as checked by numerical calculations.

8.3.2 Dependence on the number of strips

Current profiles and magnetic flux lines

The current penetration profiles for $i = 0.1, 0.2, 0.4, 0.6, 0.8$ and 0.9 for horizontal arrays with $a/b = 20$ and $d_x/a = 0.2$ are plotted for $n_{f,x} = 2$ and $n_{f,x} = 9$ in Figs.

8.8(a) and 8.8(b), respectively. The profiles for $i = 0.8$ and 0.9 are depicted in dashed lines to help the profiles identification. Fig. 8.8(a) shows the profiles for $n_{f,x} = 2$; one of the array kernels is represented by a cross. In Fig. 8.8(b) can be appreciated the full penetration of some strips for $i < 1$.

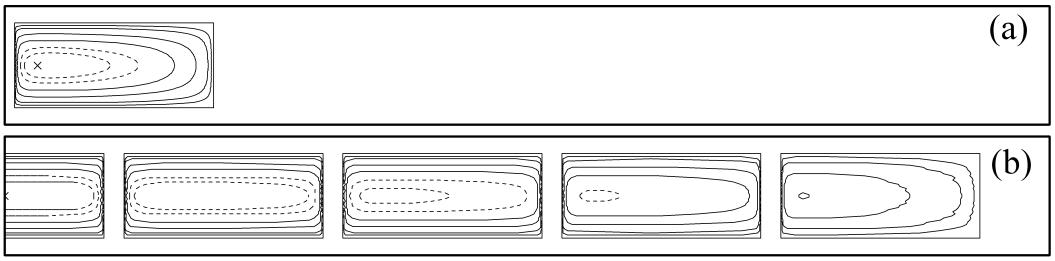

Figure 8.8: Current fronts for horizontal arrays of $n_{f,x} = 2$ (a) and 9 (b). Current profiles correspond to $i = 0.1, 0.2, 0.4, 0.6$ (solid lines) and $i = 0.8, 0.9$ (dashed lines) from outwards to inwards. The cross in (a) correspond to the kernel.

Normalized ac loss

The normalized ac loss q_t as a function of i for several number of strips $n_{f,x}$ is plotted in Fig. 8.9. As expected, the $q_t(i)$ curves present several kinks; specifically, they present $(n_{f,x} - 1)/2$ kinks if $n_{f,x}$ is odd and $(n_{f,x} - 2)/2$ if $n_{f,x}$ is even, so that each kink correspond to the full penetration of a pair of strips located symmetrically to the zy plane.

Several other features can be detected. First, the lowest loss at $i = 1$ is for $n_{f,x} = 2$. This is so because linear arrays with even $n_{f,x}$ have two kernels, which for $i = 1$ constitute the field-free core. Then, for an even number of strips the average distance from the field-free core to the current distribution, and so the vector potential difference (Fig. 8.5), is lower than for any odd number, including $n_{f,x} = 1$. Higher even number of strips have higher average distance from the kernels, so that $q_t(i = 1)$ is higher.

Second, the normalized ac loss for low i decreases with increasing the number of strips, with values that can be lower than for the thin-strip limit. As explained below, this fact occurs when i is lower than the normalized current at which the most external strip is fully penetrated. Below this current, each strip is nonsaturated with current density penetrating from the whole strip contour, including the border next to the gap (Fig.8.8). Since for high $n_{f,x}$ there is a total larger interface between the field-free core and the critical-current density region, the average vector potential difference is lower, and so is the ac loss. After some strips become fully penetrated, so that the field-free core disappears from these strips, the ac loss increases faster with i. Then, the $q_t(i)$ curve for higher $n_{f,x}$ progressively overcomes those for lower $n_{f,x}$. As a consequence, the optimum number of strips regarding the normalized ac loss depends on the reduced current at which the array is desired to operate.

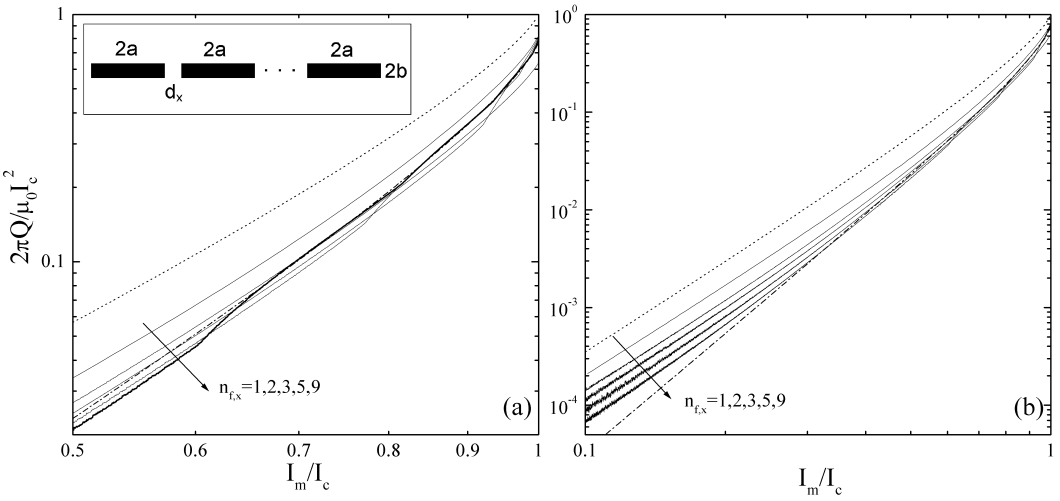

Figure 8.9: Normalized ac loss $2\pi Q_t/\mu_0 I_c^2$ as a function of the normalized ac field amplitude I_m/I_c. Solid lines correspond to horizontal arrays with $a/b = 20$, $d_x/a = 0.2$ and $n_{f,x} = 1, 2, 3, 5$ and 9 in the arrow direction (thicker line is for $n_{f,x} = 9$), dotted line is for an ellipse, calculated from Eq. (8.1), and dashed-dotted line is for a thin strip (Eq. (8.2)). Curves are plotted for i between 0.5 and 1 in (a) and between 0.1 and 1 in (b).

8.4 Vertical stacks

We next study the current distribution and transport ac loss in a set of $n_{f,x}$ rectangular strips stacked along the thin dimension of the strip with constant spacing d_y.

8.4.1 Dependence on vertical separation

Current profiles and magnetic flux lines

The current profiles at $i = 0.1, 0.2, 0.4, 0.6$ and 0.8 for a vertical stack with $a/b = 20$ are depicted for $d_y/a = 0.02$, 0.2 and 4 in Figs. 8.10(a), 8.10(b) and 8.10(c), respectively. Current profiles for vertical stacks have all the characteristics described above for horizontal arrays, with the difference that the transition from the overall behavior to the independent strip one requires higher separations in this case.

Magnetic flux lines, as well as the current profile, are plotted in Fig. 8.11 (a) and (b) corresponding to a vertical stack of three strips with $d_y/a = 0.2$ and 2, respectively, carrying a transport current of $I = 0.6 I_c$. Again, the same features as for horizontal arrays can be observed. However, the vertical stack needs a higher separation to magnetically decouple the strips. It can be seen in figure 8.11(b) how the magnetic shielding in the gap between strips is much higher than for the horizontal array with the same strip separation (Fig. 8.5).

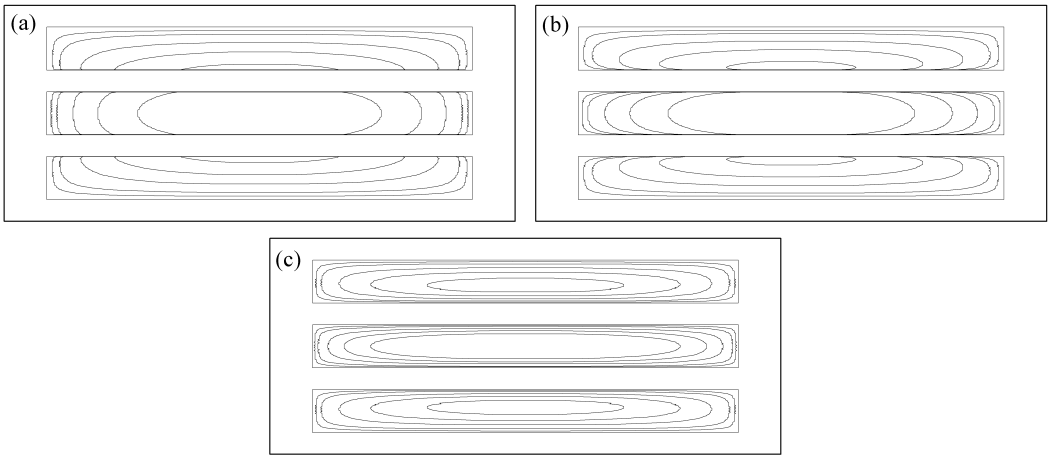

Figure 8.10: Current fronts for vertical stacks made of three strips with aspect ratio $a/b = 20$ and several vertical separations $d_y/a = 0.02$, 0.2 and 4 (a,b,c). The current fronts correspond to $i = I_m/I_c = 0.1$, 0.2, 0.4, 0.6 and 0.8 from outwards to inwards. Vertical axis has been expanded and strip separations have been drawn as the same for visualization.

Ac loss

In Fig. 8.12 we present the calculated q_t as a function of i for vertical stacks with $n_{f,y} = 3$, $a/b = 20$, and several vertical separations d_y/a. Same as for horizontal arrays, the normalized ac loss for vertical stacks shows a kink between $i = 0.9$ and 1 and below the kink it monotonically decreases with increasing strip separation. However, vertical stacks with small separation d_y/a present higher loss than for one strip, although the lowest loss is still for vertical stacks with enough high d_y/a. The reason is simply because each strip has a higher aspect ratio a/b than the vertical stack with no separation, so that the latter has higher loss than the former [79, 80, 84]. However, with increasing d_y/a the loss below the kink decreases down to $1/n_{f,y}$ times the loss for one strip (Sec. 8.3.1). We note that the loss for a densely piled vertical stack (small d_y/a) is more similar to that for a strip with a thickness equal to the sum of the thickness of the filaments than for a strip with the overall dimensions (superconducting volume plus air gaps). Another interesting issue is that the loss for stacks with $i = 1$ is higher than for a single strip for all the calculated d_y/a.

Numerical calculations have been performed for other a/b values, showing that all the above described trends and issues hold as long as $a/b \leq 20$. The case for higher aspect ratios is qualitatively different when for low d_y/a. In Fig. 8.13 we present the $q_t(i)$ curves for a vertical stack with $a/b = 50$ and vertical separations $d_y/a = 0$,0.2,2 and ∞, as well as the curve for one of the strips of the array. The only qualitative difference from Fig. 8.12 is that in Fig. 8.13 the normalized loss for $d_y/a = 0.2$ is higher than for $d_y/a = 0$ for $i \geq 0.35$, while the kink is at much higher current. The reason for this reversed trend for high a/b can be understood by means of Fig. 8.13 (inset), where

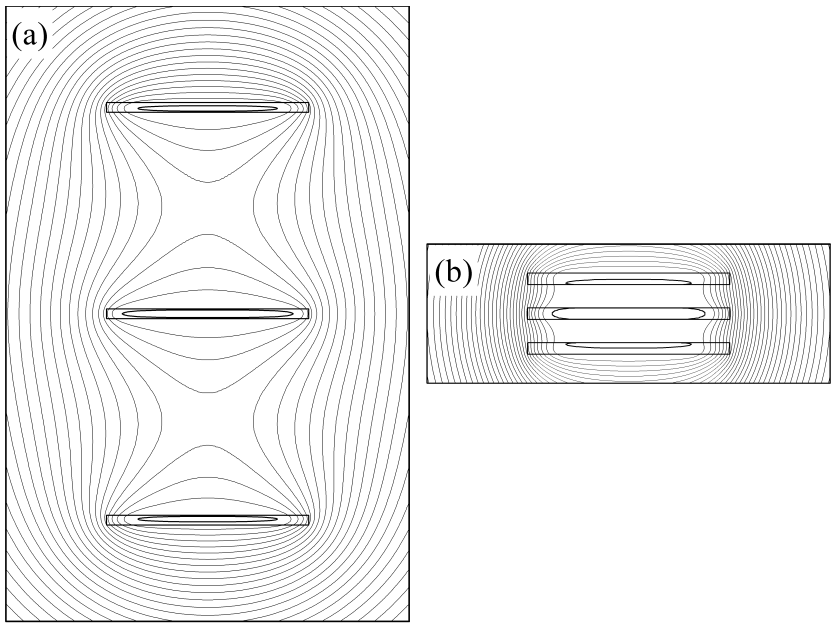

Figure 8.11: Current fronts (thick lines) and magnetic flux lines (or $A_{z,c} - A_z(\mathbf{r})$ level curves) for vertical stacks made of three strips with aspect ratio $a/b = 20$ and separation $d_y/a = 1$ (a) and $d_x/a = 0.2$ (b) carrying a transport current $I = 0.6I_c$. The $A_{z,c} - A_z(\mathbf{r})$ variation between level curves for these figures is the same as in Fig. 8.5.

the current profiles for the above mentioned cases and $i = 0.1$ and 0.6 are shown. The strips are depicted with zero separation to help the comparison. For vertical stacks with low d_y/a, the highest loss contribution comes from the current next to the outer vertical borders and the four most external corners Fig. 8.11(b), being this effect enhanced for high a/b. For $i = 0.1$, the case with $d_y/a = 0$ has deeper current penetration from the four most external corners and the vertical borders than for $d_y/a = 0.2$, so that the loss for zero separation is higher, whereas the opposite occurs for $i = 0.6$. Then, the loss for low current is lower for $d_y/a = 0.2$ than for zero separation, although for enough high current the loss for $d_y/a = 0.2$ overcome that for $d_y/a = 0$ as shown in Fig. 8.13.

8.4.2 Dependence on the number of strips

We study first the effect of stacking strips with small separation. In Fig. 8.14 we plot the normalized ac loss for vertical stacks with $a/b = 20$, $d_y/a = 0.2$ and several values of $n_{f,y}$.

The $q_t(i)$ curves in Fig. 8.14 show that the loss for low $a/b = 20$ increases with increasing the number of strips. This is because when d_y/a is low enough the array behaves almost as a single strip with aspect ratio $a/(n_{f,y}b)$ (Sec. 8.4.1); we call it the equivalent strip. Then, when increasing the number of strips, the equivalent strip aspect ratio decreases and the loss increases (Sec. 8.2.2) [84]. However, if the number of strips

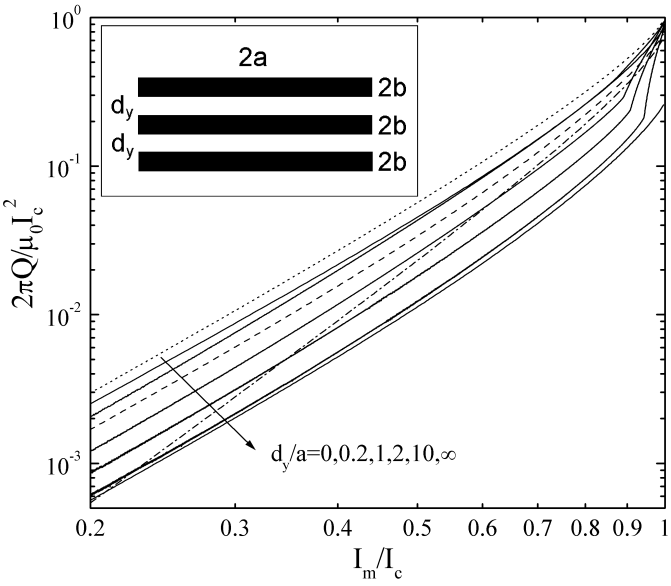

Figure 8.12: Normalized ac loss $2\pi Q_t/\mu_0 I_c^2$ as a function of I_m/I_c. Solid lines correspond to a vertical stack made of three strips with $a/b = 20$ and $d_y/a = 0, 0.2, 1, 10, \infty$ in the arrow direction, the dashed curve is for a rectangular strip with $a/b = 20$, dotted one is for the analytical formula for ellipse of Eq. (8.1), and the dash-dotted curve is for a thin strip, Eq. (8.2).

is so high that $a/(n_{f,y}b) < 1$, the tendency would be reversed since the normalized loss for a strip with a certain width-to-thickness aspect ratio γ is the same as for one with $1/\gamma$, due to the fact that the transport loss is independent of the strip orientation. As shown in Fig. 8.12, the loss of the stack is slightly lower than that for the equivalent strip for i below any kink and slightly higher than for i above, being the difference for low i more important for larger d_y/a. This deviation for low i has been confirmed for all the calculated cases in Fig. 8.14, showing that the difference in the $q_t(i)$ curves increases with increasing $n_{f,y}$. This is so because for the same change in d_y/a the average distance between one strip and the rest of strips increases more for higher number of strips, so that the mutual magnetic interaction is more reduced.

The normalized ac loss for stacks with the same strip aspect ratio, $a/b = 20$, but larger vertical separation, $d_y/a = 1$, is presented in Fig. 8.15 for several values of $n_{f,y}$. For this case, q_t decreases with $n_{f,y}$ for i below the lower kink, being this trend opposite to that for low d_y/a, Fig. 8.14. This trend appears when the strips are sufficiently magnetically decoupled, so that the governing aspect ratio comes from the strip and not from the overall. For higher i values, the outer strips subsequent penetration generates kinks in the $q_t(i)$ curve which yield to a crossover between curves for several $n_{f,y}$, as already found for horizontal strips (Sec. 8.3.2).

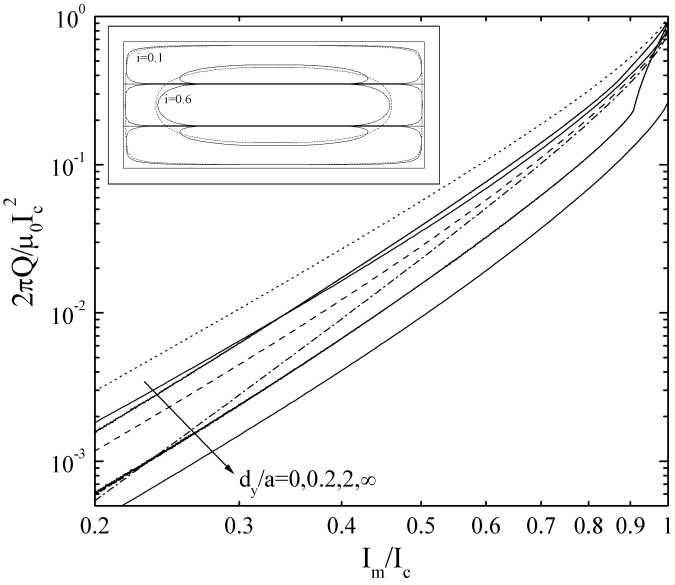

Figure 8.13: Normalized ac loss as a function of current fraction for vertical stacks with several values of the number of strips. Solid lines correspond to a vertical stack made of three strips with $a/b = 50$ and $d_y/a = 0, 0.2, 2, \infty$ in the arrow direction, the dashed curve is for a rectangular strip with $a/b = 50$, dotted one is for an ellipse, and the dash-dotted curve is for a thin strip. The inset shows the current fronts for a vertical stack with $a/b = 50$ and $d_y/a = 0.2$ (solid lines) and a rectangular strip with $a/b = 50/3$ (dotted lines). The strip separation for the array has been drawn as zero and the vertical axis has been expanded for visualization.

8.5 Matrix arrays

In this section we study the electromagnetic interaction between rectangular strips arranged in a matrix configuration, based on the results obtained for vertical and horizontal arrays.

Current profiles and magnetic flux lines

In Fig. 8.16, we present the magnetic flux lines and current profiles for matrix arrays with $a/b = 20$, $d_y/a = 0.2$ and $d_x = 0.2$ and 2 for Figs. 8.16(a) and (b), respectively. For both cases the reduced current is $i = 0.6$ and the vector potential difference between flux lines is the same. As can be seen in Fig. 8.16, the current profile and magnetic flux lines present the same issues as for horizontal and vertical stacks, Fig. 8.5 and 8.11(b).

Ac loss

The calculated ac loss for a $n_{f,x} \times n_{f,y} = 3 \times 3$ matrix array with $a/b = 20$ and several d_x/a and d_y/a separations is shown in Fig. 8.17.

In Fig. 8.17(a) we plot the $q_t(i)$ curves for a fixed $d_y/a = 0.2$ and several d_x/a.

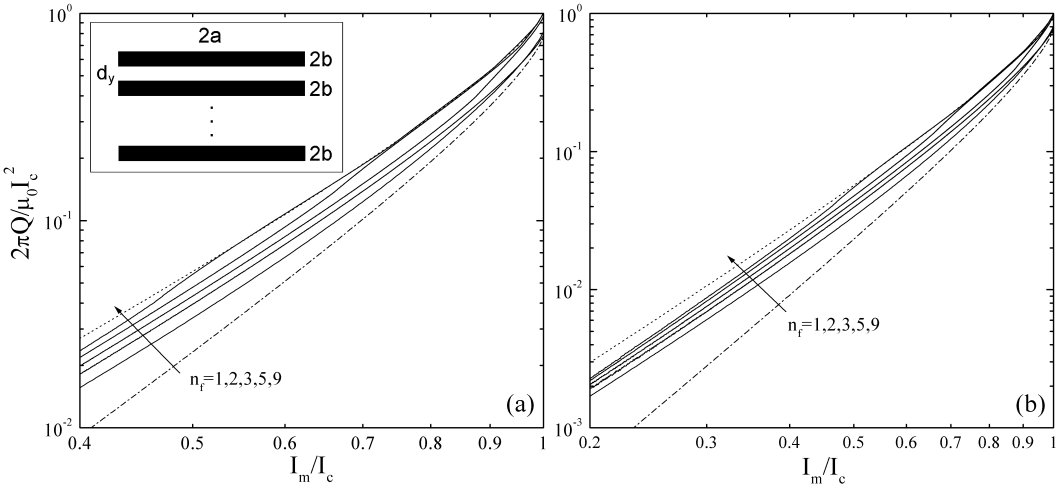

Figure 8.14: Normalized ac loss as a function of current fraction. Solid lines correspond to vertical stacks of strips with $a/b = 20$, $d_y/a = 0.2$, and $n_{f,y} = 1, 2, 3, 5, 9$ in the arrow direction. The dotted curve is for an ellipse and the dash-dotted one is for a thin strip. Curves are plotted for i between 0.4 and 1 in (a) and between 0.2 and 1 in (b).

As for horizontal arrays, the normalized ac loss monotonically decreases with increasing d_x/a down to $1/n_{f,x}$ times the loss for a column taken independently. Moreover, the loss for low d_x/a is similar to that for a vertical stack with a strip width equal to $2n_{f,x}a$. The results for the calculated case of $d_y/a = 0.2$ and $d_x/a \leq 0.2$ show that the loss for the low d_x/a and low d_y/a limit approach that for a rectangular strip with aspect ratio $n_{f,x}a/n_{f,y}b$, although it is significantly different from the loss considering the overall aspect ratio.

The effect of varying the vertical distance between strips can be illustrated by the results shown in Fig. 8.17(b), where we plot the $q_t(i)$ curves for matrices with a fixed $d_x/a = 0.2$ and several vertical distances d_y/a. The main features in this figure are the same as in Fig. 8.13. The kinks corresponding to the external strips penetration are clearly seen. The figure show that the loss for low d_y/a slightly increases with vertical separation for $i \geq 0.2$ and decreases for lower i, as can be seen from the slope at $i = 0.2$. Comparing to Fig. 8.13, the increase in q_t with increasing d_y/a for moderate i is enhanced since the electromagnetic behavior of each row is similar to that for a strip with aspect ratio $3a/b = 60$, which is higher than a/b for Fig. 8.13. Considering a further increase of d_y/a, the loss gradually decreases down to $1/n_{f,y}$ times the loss for a row of strips.

8.5.1 Comparison with experimental data

Many experiments showed that the transport ac loss in multifilamentary tapes with densely packed filaments is very similar to that for an ellipse or a thin strip, depending

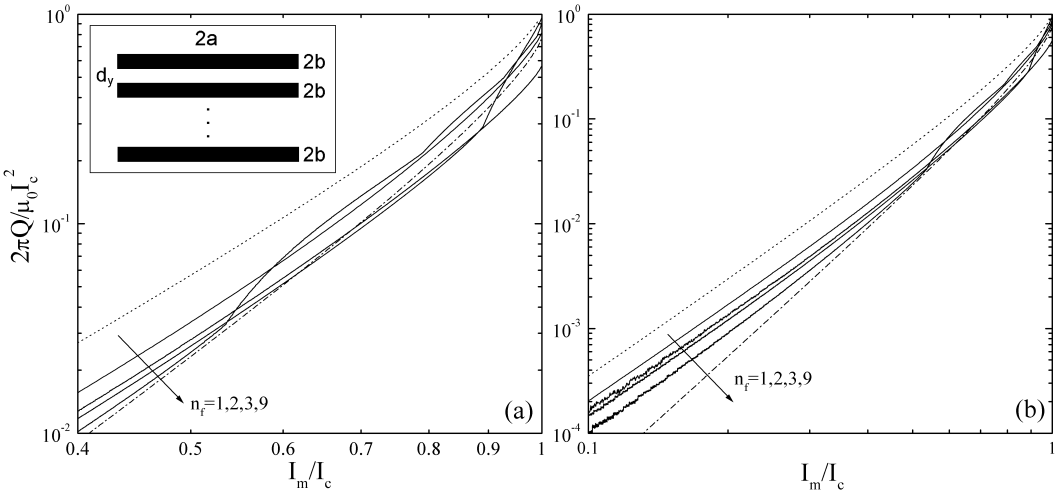

Figure 8.15: Normalized ac loss as a function of current fraction. Solid lines correspond to vertical stacks of strips with $a/b = 20$, $d_y/a = 1$, and $n_{f,y} = 1, 2, 3, 9$ in the arrow direction. The dotted curve is for an ellipse and the dash-dotted one is for a thin strip. Curves are plotted for i between 0.4 and 1 in (a) and between 0.1 and 1 in (b).

on the overall geometry [41, 36, 37, 38], being this effect consistent with the numerical data and discussion presented above for matrices.

More interesting is the measured ac loss for tapes with filaments in matrix-like arrangements, which are obtained by biaxial rolling. In Ref. [159] there are presented both experimental and numerical data for $Q_t(I)$ curves, which present a kink and are slightly lower than those for a thin strip for a certain current range. Some kinks in experimental data can also be seen in Ref. [160] for the 5×6 matrix curve with the lowest frequency. These experimental data are in agreement with the calculated results for matrices presented above.

The calculated data can also be compared to the experimental ac loss for two interacting tapes. In Refs. [156, 157] it is shown that the ac loss of the interacting tapes, either arranged vertically or horizontally, decreases with the strip separation up to the half of the loss for an independent tape. A similar feature is observed in Ref. [158]. This behavior is theoretically predicted in Secs. 8.4 and 8.3 for linear arrays of strips. Moreover, in [156] it is observed that when the two tapes are placed horizontally, the ac loss for low distances is lower than when they are placed vertically. As discussed in Secs. 8.3.1 and 8.4.1, this is due to the higher a/b overall aspect ratio, rather than to a lower magnetic coupling for the horizontal arrangement.

8.6 Chapter summary and conclusions

In this chapter we present accurate numerical results for the normalized ac loss q_t for the geometries of rectangular strips, vertical stacks, horizontal arrays and matrices.

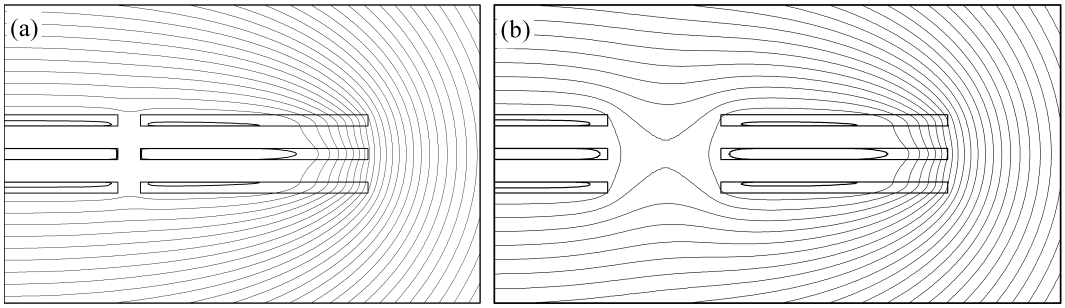

Figure 8.16: Current fronts (thick lines) and $A_{z,c} - A_z(\mathbf{r})$ level curves as magnetic flux lines for a 3×3 matrix array of strips with aspect ratio $a/b = 20$, $d_y/a = 0.2$ and $d_x/a = 0.2$ (a) and $d_x/a = 1$ (b). For both cases the array carries a transport current $I = 0.6I_c$. The $A_{z,c} - A_z(\mathbf{r})$ step between level curves for both cases is the same.

For all cases, the main features of the ac loss are carefully studied.

For rectangular strips we present an analytical formula for $q_t(i = 1)$, while the obtention of q_t for lower i needs 2D numerical calculations by means of our model of magnetic energy minimization (MEM). Such a calculations show that $q_t(i)$ monotonically decreases with increasing a/b from 1 to ∞. The 2D numerical calculations with high a/b approach the analytical formula obtained from 1D models for thin strips in [86], although they departure for low I_m. The minimum a/b value which the formula for thin strip can be used is much higher than that expected by Norris [86]. Another difference is that our numerically calculated results of q_t are proportional to i^3 for the low-i limit, in front of the i^4 dependence for thin strips.

Concerning horizontal arrays, we find that in the $q(i)$ curve there appears a change in slope (or kink) at each i value which some strips are fully penetrated by current, appearing $(n_{f,x} - 1)/2$ or $(n_{f,x}/2 - 1)$ kinks for odd or even $n_{f,x}$, respectively. These kinks are more clear for higher strip separation. For i below any kink, q_t monotonically decreases with increasing separation, decreasing down to $1/n_{f,x}$ times the loss of one of the strips for the high-separation limit. The low-separation limit corresponds to a strip with aspect ratio $n_{f,x}a/b$, being lower than one of the strips. With increasing the number of strips, q_t for i below any kink monotonically decreases, although there is a crossover for higher i. The normalized ac loss for $i = 1$ is lower for even values of $n_{f,x}$ than for odd ones due to the existence of two kernels for even $n_{f,x}$. The lowest ac loss at $i = 1$ is for $n_{f,x} = 2$.

The $q_t(i)$ curve for vertical stacks presents the same number of kinks as for horizontal ones. The normalized ac loss for $a/b \leq 20$ decreases with increasing separation for i below any kink but slightly increases for higher i. The high-separation limit is the same as for horizontal arrays. An important result is that the low-separation limit approaches more the losses of q_t for a strip with aspect ratio $a/(n_{f,y}b)$ than those for one with the aspect ratio of the overall. Then, the loss in the low-separation limit is higher than for

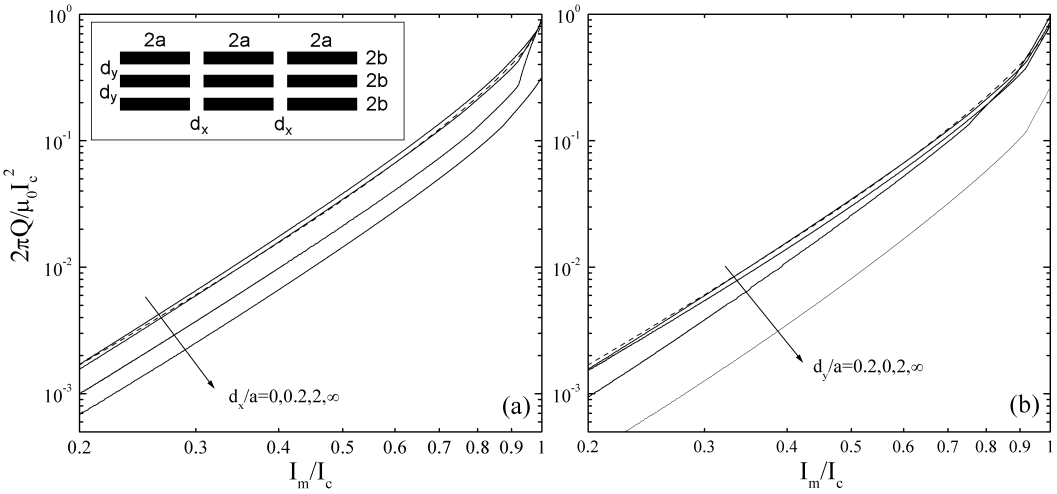

Figure 8.17: Normalized ac loss as a function of current fraction. Solid lines correspond to a 3×3 matrix array of strips with $a/b = 20$ and several strip separations. Matrices for figure (a) have the same vertical separations $d_y = 0.2$ and several horizontal ones $d_x = 0, 0.2, 2, \infty$ in the arrow direction, while for figure (b) separations are $d_x = 0.2$ and $d_y = 0.2, 0, 2, \infty$ in the arrow direction.

one of the strips in the stack. With increasing $n_{f,y}$, q_t for i below any kink increases if d_y/a is small but decreases if d_y/a is higher. For $i = 1$ the ac loss dependence on varying $n_{f,y}$ is the same as for horizontal arrays.

For matrix arrays, the behavior of q_t with varying the horizontal and vertical separation is the same as horizontal arrays and vertical stacks, respectively.

Some of these issues are also found for actual experimental situations, such as the presence of kinks in matrix arrays [159, 160] and the dependence on strip separation of two interacting strips [156, 157, 158].

Comparing to the magnetic case, we find that the magnetic coupling between strips for the transport case needs higher separations to be significantly reduced comparing to the magnetic case with isolated strips. For vertical stacks, with increasing d_y/a the magnetic ac loss Q_m increases while Q_t decreases except for $a/b > 20$ and low d_y/a, for which there is a slight increase. For horizontal arrays, with increasing d_x/a both Q_t and Q_m for isolated strips decrease, while Q_m increases for interconnected strips. The optimum case concerning magnetic ac loss in actual applications, usually working at high H_m, is the isolated strips case (Sec. 7.5.2). For this case, with increasing the horizontal separation in matrices we simultaneously decrease the transport and magnetic ac loss, while with decreasing vertical separations Q_m decreases but Q_t can increase or decrease, depending on the strips aspect ratio and their separation.

All the numerical calculations for the current profiles and q_t presented in this chapter can be also be performed for any other cross-section geometry, including more realistic irregular shapes. For the transport case, the numerical procedure for the MEM could be

easily adapted to simulate a position-dependent J_c. Much more effort would be needed to adapt the MEM procedure for to allow a $J_c(B)$ dependence.

CHAPTER 9

Conclusions

The geometry of a sample may play a very important role in its electromagnetic properties. In the first part of this thesis we have studied the geometry effects, also called demagnetizing effects, in samples made of linear homogenous isotropic materials subjected to a uniform applied magnetic field. In order to quantify the demagnetizing effects on the most relevant magnetic quantities of the samples, we have carried out accurate calculations for the fluxmetric and magnetometric demagnetizing factors, N_{f} and N_{m}, for some geometries and a wide range of susceptibility χ. In the second part of the thesis we have studied the geometry effects in hard superconductors, which are nonlinear hysteretic materials, within the critical-state model framework. For this case, we have focused on some infinitely long geometries subjected to either a transverse ac applied field or a transport alternating current with amplitudes H_m and I_m, respectively. An interesting quantity for these cases is the ac loss, for which numerical calculations have been presented and discussed.

For linear materials, we detected there were some important lacks in the published calculations of the demagnetizing factors for the most interesting geometries of rectangular prisms and cylinders. In order to fill some of these lacks, we have presented accurate numerical calculations for a wide range of susceptibility χ values and aspect ratio/s for infinitely long rectangular bars and square bars, as well as for perfectly shielded rectangular prisms. These calculations have been done by a numerical method developed in this thesis, based on an already existing method for cylinders in axial applied field. This numerical method is ready to calculate $N_{\mathrm{f,m}}$ for the general case of rectangular prisms with arbitrary susceptibility and results will be published elsewhere. For the development of the numerical method it has been useful the derivation of exact analytical formulae of the surface pole density σ for $\chi = \infty$. From $\sigma(\chi = \infty)$ we have rederived the exact analytical results of $N_{\mathrm{f,m}}$ for $\chi = \infty$ and N_{m} for $\chi = -1$ and have found

an analytical approximation for $N_{\rm f}(\chi = -1)$. These analytical results, together with existing ones for $\chi = 0$, have also been very useful for the development of the numerical method. Besides, we have found a relation for cylinders between $N_{\rm m}$ with field applied in the radial direction ($N_{\rm m}^r$) and $N_{\rm m}$ in the axial one ($N_{\rm m}^a$), and used it to calculate $N_{\rm m}^r$ from existing results of $N_{\rm m}^a$.

A systematic study of infinitely long hard superconductors with transverse applied field or carrying transport current has been done for the infinite geometries of rectangular bars (strips), elliptical bars, and some regular arrangements of strips, such as vertical stacks, horizontal arrays, matrices, and interleaved arrays. This study have been done by numerical calculations using a method based on the critical-state model and magnetic energy minimization (MEM).

For the magnetic case, we have considered the two different situations of strips mutually electrically isolated or interconnected at infinity, situations which present very different magnetic behavior for horizontal arrays, matrices, and interleaved arrangements. The magnetic quantities calculated and discussed are current profiles, magnetization, ac susceptibility, and magnetic ac loss Q_m. An interesting feature for isolated strips is the presence of magnetic flux compression in the horizontal separation between strips. For this interconnected strip case, there appear some interesting issues concerning the imaginary part of the ac susceptibility χ'', proportional to Q_m/H_m^2, specifically for the height and the width of the $\chi''(H_m)$ peak. We have also showed that the magnetic behavior for a matrix is qualitatively the same as for vertical stacks and horizontal arrays concerning strip separation and number of strips in the vertical and horizontal directions, respectively. For the isolated case, we have compared $\chi''(H_m)$ for a matrix to that for interleaved arrangements, showing that matrices present lower values of χ'', and therefore lower ac loss, for the ac field amplitudes near the peak in χ''. Another interesting issue is that for rectangular strips the low-H_m limit for χ'', is proportional to H_m for any thickness-to-width aspect ratio, a result which is extensible to any two-dimensional cross-section.

The transport case for the geometries of rectangular strips, horizontal arrays, vertical stacks and matrices has been also systematically studied, obtaining some interesting features. First, we have found that horizontal arrays and vertical stacks with an even number of strips present two kernels in the two strips closer to the overall geometrical center. As a consequence, arrangements with an even number of strips present lower losses at critical current than those with an odd number. Similar features have been found for matrices, with the particularity that they can also present four kernels if both the number of strips in the vertical and horizontal directions are even. We have found that the magnetic coupling between strips for the transport case decreases with increasing strip separation, although the transport case needs higher separations to be significantly reduced as compared to the magnetic case with isolated strips. Concerning the normalized ac loss q_t, calculations for different arrangements of strips show that the $q_t(I_m)$ curve presents some points with sudden increase of the slope (kink), corresponding to the full penetration of a strip of the arrangement.

From the results of magnetic and transport ac loss we can extract some trends that can be used to reduce ac loss in actual superconducting tapes. The ac loss for rectangular prisms with a width-to-thickness aspect ratio γ always increase with increasing γ for the magnetic case with applied field parallel to the thickness. However for the transport case the ac loss decreases for $\gamma > 1$ and increases for $\gamma < 1$. As to the optimum arrangement of strips, the situation of isolated strips presents lower magnetic ac loss than the interconnected one for moderate and high H_m, which is the range of H_m that most applications operate. For isolated strips, with increasing horizontal separation in matrix arrays one can simultaneously decrease the transport and magnetic ac loss, whereas with decreasing vertical separations Q_m decreases but Q_t can increase or decrease, depending on the strips aspect ratio and their separation. For both isolated and interconnected cases, with increasing the number of strips in the horizontal direction Q_m increases but Q_t decreases, whereas with increasing the number of strips in the vertical direction Q_t may increase or decrease depending on the strip separation and Q_m always decrease.

The most important results of this thesis have been obtained by means of two numerical procedures, one for demagnetizing factors in LHI materials (chapter 3) and the other for transverse properties of infinitely long hard superconductors (chapter 6). The procedure for demagnetizing factors developed for the general case of finite rectangular prisms with arbitrary susceptibility can eventually be applied to a set of several rectangular prisms with different susceptibility, describing the interaction between different LHI materials, as in a magnetic or superconducting multilayer. Besides, the procedure for hard superconductors with multifilamentary configuration allows to be applied to more realistic cross-sections in order to better simulate actual superconducting tapes. The model may also be extended to nonuniform critical-current densities or nonuniform applied fields. An interesting extension of the MEM procedure would be to consider the response to an applied ac field acting simultaneously with a transport alternating current.

We hope that the work presented in this thesis will be useful for the future development and understanding of magnetic materials and superconductors. A part of this thesis is dedicated to reduce the energy loss in superconducting tapes and wires, the appropriate use of which can contribute to the reduction of energy production, and hence, a more sustainable development for the future.

Bibliography

[1] J. C. Maxwell, *A Treatise on Electricity and Magnetism* (third edition), vol. 2, Oxford: Claredon, 1892, pag. 66-73. First edition: 1873. Reprinted New York: Dover, 1954.

[2] T. L. Templeton and A. S. Arrott, IEEE Trans. Magn. **MAG-23**, 2650 (1987).

[3] D. X. Chen, J. A. Brug, and R. B. Goldfarb, IEEE Tans. Magn. **27**, 3601 (1991).

[4] M. Kobayashi and Y. Ishikawa, IEEE Trans. Magn. **28**, 1810 (1992).

[5] M. Kobayashi, Y. Ishikawa, and S. Kato, IEEE Trans. Magn. **32**, 254 (1996).

[6] F. M. Araujo-Moreira, C. Navau, and A. Sanchez, Phys. Rev. B **61**, 634 (2000).

[7] C. P. Bean, Phys. Rev. Lett. **8**, 250 (1962).

[8] C. P. Bean, Rev. Mod. Phys. **36**, 31 (1964).

[9] H. London, Phys. Lett. **6**, 162 (1963).

[10] J. R. Reitz, F. J. Milford, and R. W. Christy, *Foundations of the Electromagnetic Theory* (Reading [Mass.]: Addison-Wesley, 1979).

[11] J. D. Jackson, *Classical Electrodynamics* (New York: John Wiley & Sons, 1975).

[12] L. D. Landau, E. M. Lifshitz, and L. P. Pitaevskii, *Electrodynamics of Continuous Media* (Oxford: Pergamon Press, 1984).

[13] E. Pardo, A. Sanchez, and D.-X. Chen, J. Appl. Phys. **91**, 5260 (2002).

[14] B. D. Cullity, *Introduction to Magnetic Materials*, (Reading [Mass.]: Addison-Wesley, 1972).

[15] E. Schlömann, J. Appl. Phys. **33**, 2825 (1962).

[16] R. A. Hein, T. L. Francavilla, D. H. Liebenberg, eds. *Magnetic Susceptibility of Superconductors and Other Spin Systems* (New York: Plenum, 1991).

[17] F. Gömöry, Supercod. Sci. Technol. **10**, 523 (1997).

[18] W. F. Brown, Jr., *Magnetostatic Principles in Ferromagnetism*, (Amsterdam: North-Holland, 1962).

[19] W. F. Brown, Jr. and A. H. Morrish, Phys. Rev. **105**, 1198 (1957).

[20] R. Moskovitz and E. Della Torre, IEEE Tans. Magn. **MAG-2**, 739 (1966).

[21] A. C. Rose-Innes and E. H. Rhoderik, *Introduction to Superconductivity* (Oxford: Pergamon Press, 1969).

[22] P. G. de Gennes, *Superconductivity of Metals and Alloys* (Reedwod City: Addison-Wesley, 1989).

[23] C. P. Poole Jr, H. A. Farach, and R. J. Creswick, *Superconductivity* (San Diego: Academic Press, 1995).

[24] D.-X. Chen, J. J. Moreno, A. Hernando, A. Sanchez, and B.-Z. Li, Phys. Rev. B **57**, 5059 (1998).

[25] D.-X. Chen and R. B. Goldfarb, J. Appl. Phys **66**, 2489 (1989).

[26] D.-X. Chen, A. Sanchez, J. Nogués, and J.S. Muñoz, Phys. Rev. B **41**, 9510 (1990).

[27] A. Sanchez, Physica C **255**, 136 (1994).

[28] R. B. Godfarb, M. Lelental, C. A. Thompson, in *Magnetic Susceptibility of Superconductors and Other Spin Systems*, eds. R. A. Hein, T. L. Francavilla, D. H. Liebenberg (New York: Plenum, 1991).

[29] D.-X. Chen and A. Sanchez, J. Appl. Phys. **70**, 5463 (1991).

[30] Y. Fukumoto, H. J. Wiesmann, M. Garber, M. Suenaga, and P. Haldar, Appl. Phys. Lett. **67**, 3180 (1995).

[31] M. Suenaga, V. F. Solovyov, Q. Li, Z. Ye, H. J. Wiesmann, M. Iwakuma, M. Fukui, K. Toyota, F. Funaki, T. H. Johansen, D. V. Shantsev, and J. R. Clem, J. Appl. Phys **94**, 502 (2003).

[32] F. Gömöry, R. Tebano, A. Sanchez, E. Pardo, C. Navau, I. Husek, F. Strycek, and P. Kovac, Supercond. Sci. Technol. **15**, 1311 (2002).

[33] E. Pardo, A. Sanchez, C. Navau, F. Gömöry, I. Husek, F. Strycek, R. Tebano, and P. Kovac, Physica C **372-376**, 1788 (2002).

[34] A. Palau, T. Puig, X. Obradors, E. Pardo, C. Navau, A. Sanchez, A. Usoskin, H. C. Freyhardt, L. Fernández, B. Holzapfel, R. Feenstra, Appl. Phys. Lett **84**, 230 (2004).

[35] D. R. Salmon and J. A. Caterall, J. Phys. D: Appl. Phys. **3**, 1023 (1970).

[36] M. Majoros, L. Jansak, S. Zannella, F. Curcio, P. La Cascia, V. Ottoboni, C. M. Friend, L. Le Lay, B. A. Glowacki, and A. M. Campbell, Physica C **310**, 6 (1998).

[37] A. Oota, T. Fukunaga, M. Matsui, S. Yuhya, and M. Hiraoka, Physica C **249**, 157 (1995).

[38] F. Gömöry, L. Gherardi, R. Mele, D. Morin, and G. Crotti, Physica C **279**, 39 (1997).

[39] Y. Yang, T. Hughes, C. Beduz, D. M. Spiller, R. G. Scurlock, and W. T. Norris, Physica C **256**, 378 (1996).

[40] Y. Yang, T. J. Hughes., E. Martinez, and C. Beduz, IEEE Trans. Appl. Supercond. **9**, 1177 (1999).

[41] C. M. Friend, S. A. Awan, L. Le Lay, S. Sali, T. P. Beales, Physica C **279**, 145 (1997).

[42] S. Stavrev and B. Dutoit, Physica C **310**, 86 (1998).

[43] H. Eckelmann, M. Quilits, M. Oomen, M. Leghissa, and W. Goldacker, Physica C **310**, 122 (1998).

[44] Y. B. Kim, C. F. Hempstead, and A. R. Strnad, Phys. Rev. Lett. **9**, 306 (1962).

[45] W. A. Fietz, M. R. Beasley, J. Silcox, and W. W. Webb, Phys. Rev. **136**, A335 (1964).

[46] J. H. P. Watson, J. Appl. Phys. **39**, 3406 (1968).

[47] D.-X. Chen, A. Sanchez, and J. S. Muñoz, J. Appl. Phys. **67**, 3430 (1990).

[48] F. Gömöry and L. Gherardi, Physica C **280**, 151 (1997).

[49] D.-X. Chen, A. Sanchez, and E. Pardo, Supercond. Sci. Technol. **17**, 256 (2004).

[50] R. Inada, A. Oota, and H. Fujimoto, Physica C **378-381**, 1133 (2002).

[51] C. Romero-Salazar and F. Pérez-Rodríguez, Supercond. Sci. Technol. **16**, 1273 (2003).

[52] E. Pardo, D.-X. Chen, and A. Sanchez, to be published in IEEE Trans. on Magn.

[53] E. Pardo, D.-X. Chen, and A. Sanchez, to be published in J. Appl. Phys.

[54] D.-X. Chen, C. Prados, E. Pardo, A. Sanchez, and A. Hernando, J. Appl. Phys. **91**, 5254 (2002).

[55] D.-X. Chen, E. Pardo, and A. Sanchez, IEEE Trans. Magn. **37**, 3877 (2001).

[56] D.-X. Chen, E. Pardo, and A. Sanchez, IEEE Trans. Magn. **38**, 1742 (2002).

[57] E. C. Stoner, Phil. Mag., ser. 7 **36**, 803 (1945).

[58] J. A. Osborn, Phys. Rev. **67**, 351 (1945).

[59] R. I. Joseph, J. Appl. Phys. **37**, 4639 (1966).

[60] W. F. Brown, Jr., Am. J. Phys. **28**, 542 (1960).

[61] T. T. Taylor, J. Res. Nat. Bur. Standards **64B**, 135 (1960).

[62] T. T. Taylor, J. Res. Nat. Bur. Standards **64B**, 199 (1960).

[63] D.-X. Chen, J. Appl. Phys. **89**, 3413 (2001).

[64] E. H. Brandt and G. P. Mikitik, Phys. Rev. Lett. **85**, 4164 (2000).

[65] E. Pardo, *Factors de Desimantació de Prismes Rectangulars Infinits i de Cilindres*, Research work report (http://asimov.uab.es/cocoon/profe/epardov/index.htm).

[66] P. Rhodes and G. Rowlands, Proc. Leeds Phil. Lit. Soc. **6**, 191 (1954).

[67] F. M. Araujo-Moreira, O. Florencio, C. Navau, E. Pardo, and A. Sanchez, Physica C **341-348**, 2055 (2000).

[68] P. Fabbricatore, S. Farinon, S. Innoceti, and F. Gömöry, Phys. Rev. B **61**, 6413 (2000).

[69] S. Farinon, P. Fabbricatore, F. Gömöry, and E. Seiler, IEEE Trans. Appl. Supercond. **11**, 2776 (2001).

[70] E. Pardo, A. Sanchez, and C. Navau, IEEE Trans. Appl. Supercond. **13**, 3566 (2003).

[71] E. Pardo, A. Sanchez, and C. Navau, Phys. Rev. B **67**, 104517 (2003).

[72] A. Sanchez and C. Navau, Phys. Rev. B, **64**, 214506 (2001).

[73] C. Navau and A. Sanchez, Phys. Rev. B, **64**, 214507 (2001).

[74] A. Sanchez and C. Navau, Supercond. Sci. Technol. **14**, 444 (2001).

[75] L. Prigozhin, J. Comp. Phys. **129**, 190 (1996).

[76] L. Prigozhin, IEEE Trans. Appl. Supercond. **7**, 3866 (1997).

[77] A. Badia, C. Lopez, and J. L. Giordano, Phys. Rev. B **58**, 9440 (1998).

[78] A. Badia and C. Lopez, Phys. Rev. Lett. **87** 127004 (2001).

[79] T. Fukunaga, R. Inada, and A. Oota, Appl. Phys. Lett. **72**, 3362 (1998).

[80] M. Däumling, Supercond. Sci. Technol. **11**, 590 (1998).

[81] A. Badia and C. Lopez, Phys. Rev. B **65**, 104514 (2002).

[82] P. Chaddah, Pranama- J. Phys. **36**, 353 (1991).

[83] K. V. Bhagwat, S. V. Nair, and P. Chaddah, Physica C **227**, 176 (1994).

[84] E. Pardo, D.-X. Chen, A. Sanchez, and C. Navau, Supercond. Sci. Technol. **17**, 83 (2004).

[85] E. Pardo, D.-X. Chen, A. Sanchez, and C. Navau, Supercond. Sci. Technol. **17**, 537 (2004).

[86] W. T. Norris, J. Phys. D: Appl. Phys. **3**, 489 (1970).

[87] E. H. Brandt, M. V. Indebom, and A. Forkl, Europhys. Lett. **22**, 735 (1993).

[88] E. H. Brandt, Phys. Rev. B **54**, 4246 (1996).

[89] J. R. Clem and A. Sanchez, Phys. Rev. B **50**, 9355 (1994).

[90] E. H. Brandt, Phys. Rev. B **58**, 6506 (1998).

[91] D. Karmakar and K. V. Bhagwat, Phys. Rev. B **65**, 024518 (2001).

[92] Y. Mawatari, Phys. Rev. B **54**, 13215 (1996).

[93] D.-X. Chen, J. Nogues, and K. V. Rao, Cryogenics **29**, 800 (1989).

[94] E. Pardo, A. Sanchez, D.-X. Chen, and C. Navau, *Theoretical analysis of the transport critical-state ac loss in arrays of superconducting rectangular strips*, preprint.

[95] W. H. Press, S. A. Teukolsky, W. T. Vetterling, and B. P. Flannery, *Numerical Recipies in C*, Cambridge University Press, 1992.

[96] A. Sanchez and C. Navau, IEEE Trans. Appl. Supercond. **9**, 2195 (1999).

[97] A. Sanchez and C. Navau, Physica C **364-365**, 360 (2001).

[98] C. Navau and A. Sanchez, IEEE Trans. Appl. Supercond. **9**, 1610 (1999).

[99] C. Navau and A. Sanchez, Supercond. Sci. Technol. **15**, 1445 (2002).

[100] C. Navau and A. Sanchez, Physica C **372-376**, 1474 (2002).

[101] C. Navau, A. Sanchez, and E. Pardo, IEEE Trans. Appl. Supercond. **13**, 2185 (2003).

[102] C. Navau, A. Sanchez, E. Pardo, and D.-X. Chen, *Superconducting levitation with different cooling heights*, preprint.

[103] C. Navau, A. Sanchez, E. Pardo, and D.-X. Chen, to be published in Supercond. Sci. Technol.

[104] T. Puig, A. Palau, X. Obradors, E. Pardo, C. Navau, A. Sanchez, Ch. Jooss, K. Guth, and H.C. Freyhardt, *Identification of grain-boundary networks of distinct critical current density in* $YBa_2Cu_3O_{7-x}$ *coated conductors*, preprint.

[105] A. Palau, T. Puig, X. Obradors, A. Usoskin, H. Freyhardt, L. Fernandez, B. Holzapfel, R. Feenestra, A. Sanchez, and E. Pardo, to be published in Physica C.

[106] J. R. Hull, Rep. Prog. Phys. **66**, 1865 (2003).

[107] D. Larbalestier, A. Gurevich, D. M. Feldmann, and A. Polyanskii, Nature **414**, 368 (2001).

[108] M. P. Oomen, R. Nanke, and M. Leghissa, Supercond. Sci. Technol. **16**, 339 (2003).

[109] P. Vase, R. Flukiger, M. Leghissa, and B Glowacki, Supercond. Sci. Technol. **13**, R71 (2000).

[110] A. P. Malozemoff, D. T. Verebelyi, S. Fleshler, D. Aized, and D. Yu, Physica C **386**, 424 (2003).

[111] G. Ries, M. Leghissa, J. Rieger, J. Wiezorek, and M. Oomen, Physica C **310**, 283 (1998).

[112] M. N. Wilson, *Superconducting Magnets*, Oxford Univ. Press, Oxford, 1983.

[113] W. J. Carr, Jr., *ac Loss and Macroscopic Theory of Superconductors*, Gordon & Breach Sci. Publishers Inc., New York, 1983.

[114] K.-H. Müller, Physica C **312**, 149 (1999).

[115] M. P. Oomen, J. Rieger, and M. Leghissa, Appl. Phys. Lett. **70**, 3038 (1997).

[116] A. Wolfbrandt, N. Magnusson, and S. Hörnfeldt, IEEE Trans. Appl. Supercond. **11**, 4123 (2001).

[117] T. Chiba, Q. Li, S. P. Ashworth, and M. Suenaga, IEEE Trans. Appl. Supercond. **9**, 2143 (1999).

[118] A. Oota, T. Fukunaga, T. Abe, S. Yuhya, and M. Hiraoka, Appl. Phys. Lett. **66**, 2128 (1995).

[119] A. V. Volkozub, J. Everett, G. Perkins, P. Buscemi, A. D. Caplin, M. Dhallé, F. Marti, G. Grasso, Y. B. Huang, and R. Flükiger, IEEE Trans. Appl. Supercond. **9**, 2147 (1999).

[120] A. V. Volkozub, A. D. Caplin, Y. B. Huang, R. Flükiger, G. Grasso, H. Eckelmann, M. Quilitz, W. Goldacker, Physica C **310**, 159 (1998).

[121] J. Everett, G. Perkins, A. V. Volkozub, A. D. Caplin, M. Dhallé, A. Polcari, F. Marti, Y. B. Huang, and R. Flükiger, Physica C **310**, 202 (1998).

[122] S. P. Ashworth, B. A. Glowacki, M. Ciszek, E. C. L. Chesneau, and P. Haldar, IEEE Trans. Appl. Supercond. **7**, 1662 (1997).

[123] B. A. Glowacki, C. J. van der Beek, and M. Konczykowski, Inst. Phys. Conf. Ser. **167**, vol. 2, 779 (2000).

[124] F. Gömöry, L. Gherardi, G. Crotti, D. Bettinelli, L. Martini, L. Bigoni, and S. Zannella, Physica C **310**, 168 (1998).

[125] A. V. Bobyl, D. V. Shantsev, T. H. Johansen, M. Baziljevick, Y. M. Galperin, and M. E. Gaevski, Supercond. Sci. Technol. **13**, 183 (2000).

[126] C. J. Clem, in *Magnetic Susceptibility of Superconductors and Other Spin Systems*, eds. R. A. Hein, T. L. Francavilla, D. H. Liebenberg (New York: Plenum, 1991).

[127] E. H. Brandt, Phys. Rev. B **48**, 12893 (1993).

[128] E. H. Brandt, Phys. Rev. B **49**, 9024 (1994).

[129] E. Zeldov, J. R. Clem, M. McElfresh, and M. Darwin, Phys. Rev. B **49**, 9802 (1994).

[130] Y. Mawatari, IEEE Trans. Appl. Supercond. **7**, 1216 (1997).

[131] R. M. Ainbinder and G. M. Maksimova, Supercond. Sci. Technol. **16**, 871 (2003).

[132] R. Tebano, F. Gömöry, E.Seiler, F. Stryceck, Physica C **372-376**, 998 (2002).

[133] S. Stavrev, B. Dutoit, and P. Lombard, Physica C **384**, 19 (2003).

[134] S. Stavrev, B. Dutoit, and P. Lombard **13**, 3561 (2003).

[135] A. Forkl, Phys. Scr. **T49**, 148 (1993).

[136] Y. E. Kuzovlev, JETP Lett. **61**, 1000 (1995).

[137] K. V. Bhagwat and D. Karmakar, Europhys. Lett. **49**, 715 (2000).

[138] D. Karmakar and K. V. Bhagwat, Physica C **398**, 20 (2003).

[139] A. Sanchez, E. Pardo, C. Navau and D.-X. Chen, *Effect of filament arrangement on the magnetic ac losses of superconducting tapes*, preprint.

[140] E. H. Brandt, Phys. Rev. B **55**, 14513 (1997).

[141] V. Ivaska, V. Jonkus, and V. Palenskis, Physica C **319**, 79 (1999).

[142] G. P. Mikitik and E. H. Brandt, Phys. Rev. B **64**, 092502 (2001).

[143] A. A. B. Brojeny and J. R. Clem, Phys. Rev. B **68**, 174514 (2003).

[144] E. Pardo, D.-X. Chen, A. Sanchez, and C. Navau, to be published in Inst. Phys. Conf. Ser.

[145] F. Gömöry, J. Šouc, A. Laudis, P. Kováč, and I. Hušek, Supercond. Sci. Technol. **13**, 1580 (2000).

[146] F. Gömöry, J. Šouc, P. Fabbricatore, S. Farinon, F. Strýček, P. Kováč, and I. Hušek, Physica C **371**, 229 (2002).

[147] M. Suenaga, T. Chiba, S. P. Ashworth, D. O. Welch, and T. G. Holesinger, J. Appl. Phys. **88**, 2709 (2000).

[148] M. Suenaga, Physica C **372-376**, 1730 (2002).

[149] M.P. Oomen, J.J. Rabbers, B. ten Haken, J. Rieger, M. Leghissa, Physica C **361**, 144 (2001).

[150] Th. Herzog, H. A. Radovan, P. Ziemann, and E. H. Brandt, Phys. Rev. B **56**, 2871 (1997).

[151] T. Fukunaga, T. Abe, A. Oota, S. Yuhya, and M. Hiraoka, Appl. Phys. Lett. **66**, 2128 (1995).

[152] M. Leghissa, B. Gromoll, J. Rieger, M. Oomen, H.-W. Neumüller, R. Schlosser, H. Schmidt, W. Knorr, M. Meinert and U. Henning, Physica C **372-376**, 1688 (2002).

[153] L. Gherardi, F. Gömöry, R. Mele, and G. Coletta, Supercond. Sci. Technol. **10**, 909 (1997).

[154] M. Majoros, B. A. Glowacki, and A. M. Campbell, Physica C **334**, 129 (2000).

[155] A. Melini, R. Tebano, and R. Mele, Physica C **340**, 308 (2000).

[156] T. J. Hughes, Y. Yang, C. Beduz, and A. Power, Physica C **310**, 187 (1998).

[157] T. J. Hughes, Y. Yang, C. Beduz, and A. Power, IEEE Trans. Appl. Supercond. **9**, 774 (1999).

[158] S. Choi, D. Kim, W. Nah, J. Joo, J. Jung, and K. Ryu, Physica C **372-376**, 1746 (2002).

[159] A. Oota, R. Inada, N. Inagaki, P. X. Zhang, and H. Fujimoto, Physica C **386**, 100 (2003).

[160] M. Dhalle, A. Polcari, F. Marti, Y. B. Huang, G. Witz, and R. Flükiger, IEEE Trans. Appl. Supercond. **9**, 782 (1999).

[161] F. Gömöry, J. Šouc, P. Fabbricatore, S. Farinon, F. Strýček, P. Kováč, and I. Hušek, Physica C **371**, 229 (2002).

[162] D.-X. Chen, E. Pardo, and A. Sanchez, Supercond. Sci. Technol. **17**, 16 (2004).

[163] R. Hancox, Proc. IEE **113**, 1221 (1966).

[164] K.-H. Müller, Physica C **289**, 123 (1997).

[165] W. T. Norris, J. Phys. D: Appl. Phys. **4**, 1358 (1971).

[166] T. Fukunaga, R. Inada, and A. Oota, IEEE Trans. Appl. Supercond. **9**, 1057 (1999).

[167] J. Rhyner, Physica C **310**, 42 (1998).

[168] T. Yazawa, J. J. Rabbers, B. ten Haken, H. H. J. ten Kate, and H. Maeda, J. Appl. Phys. **84**, 5652 (1998).

[169] S. Stavrev, B. Dutoit, and F. Grilli, IEEE Trans. Appl. Supercond. **13**, 3807 (2003).

[170] J. Rhyner, Physica C **310**, 42 (1998).

[171] J. Lehtonen, M. Ahoranta, and R. Mikkonen, Physica C **372-376**, 1743 (2002).

List of publications by Enric Pardo

1. 'AC and DC magnetization of finite cylindrical and orthorombic superconductors'
   F.M. Araujo-Moreira, O. Florencio, C. Navau, E. Pardo, and A. Sanchez
   Physica C **341-348**, 2055 (2000)

2. 'Radial Magnetometric Demagnetizing Factor of Thin Disks'
   D.-X. Chen, E. Pardo, and A. Sanchez
   IEEE Trans. on Magn. **37**, 3877 (2001)

3. 'Transverse Demagnetizing Factors of Long Rectangular Bars: I. Analytical Expressions for Extreme Values of Susceptibility'
   D.-X. Chen, C. Prados, E. Pardo, A. Sanchez, and A. Hernando
   J. Appl. Phys. **15**, 5254 (2002)

4. 'Transverse Demagnetizing Factors of Long Rectangular Bars: II. Numerical Calculations for Arbitrary Susceptibility'
   E. Pardo, A. Sanchez, D.-X. Chen
   J. Appl. Phys. **15**, 5260 (2002)

5. 'Demagnetizing factors of rectangular prisms and ellipsoids'
   Du-Xing Chen, Enric Pardo and Alvaro Sanchez
   IEEE Trans. on Magn. **38**, 1742 (2002).

6. 'Current profiles and AC losses of a superconducting strip with elliptic cross-section in perpendicular magnetic field'
   F. Gomory, R. Tebano, A. Sanchez, E. Pardo, C. Navau, I. Husek, F. Strycek and P.Kovac
   Supercond. Sci. Technol. **15**, 1311 (2002).

7. 'Critical current and AC susceptibility in superconducting tapes with elliptical cross-section'
   E. Pardo, A. Sanchez, C. Navau, F. Gömöry, I. Husek, F. Strycek, R. Tebano, P.

Kovac
Physica C **372-376**, 1788 (2002).

8. 'Magnetic properties of arrays of superconducting strips in perpendicular field'
E. Pardo, A. Sanchez, and C. Navau
Phys. Rev. B **67**, 104517 (2003).

9. 'Theoretical AC susceptibility of superconducting multifilamentary tapes in a perpendicualar field'
E. Pardo, A. Sanchez, and C. Navau
IEEE Trans. Appl. Supercond. **13**, 3566 (2003).

10. 'Lateral force in permanent magnet-superconductor levitation systems with high critical current'
C. Navau, A. Sanchez, and E. Pardo
IEEE Trans. Appl. Supercond. **13**, 2185 (2003).

11. 'Transport AC loss in a long cylinder with hard superconducting core and normal conducting shell'
D.-X. Chen, E. Pardo and A. Sanchez
Supercond. Sci. Technol **17**, 16 (2004).

12. 'Alternating current loss in rectangular superconducting bars with a constant critical-current density'
E. Pardo, D.-X. Chen, A. Sanchez, and C. Navau
Supercond. Sci. Technol. **17**, 83 (2004).

13. 'Transport AC loss of superconducting cylinder with field and radius dependent critical-current density'
D.-X. Chen, A. Sanchez and E. Pardo
Supercond. Sci. Technol. **17**, 256 (2004).

14. 'Simultaneous inductive determination of grain and inter-grain critical current densities of $YBa_2Cu_3O_{7-x}$ coated conductors'
A. Palau, T. Puig, X. Obradors, E. Pardo, C. Navau, A. Sanchez, A. Usoskin, H.C. Freyhardt, L. Fernández, B. Holzapfel, R. Feenstra
Appl. Phys. Lett. **84**, 230 (2004).

15. 'Transverse critical-state susceptibility of rectangular bars'
E. Pardo, D.-X. Chen, A. Sanchez, and C. Navau
Supercond. Sci. Technol. **17**, 537 (2004).

16. 'Influence of filament arrangement on current distribution and AC loss in Bi-2223/Ag tapes'
F. Gömöry, E. Seiler, J. Šouc, S. Farinon, P. Fabbricatore, G. Perkins, A.D. Caplin,

E. Pardo, A. Sanchez, C. Navau
Supercond. Sci. Technol. **17**, S150 (2004).

17. 'Demagnetizing Factors for Square Bars'
E. Pardo, D.-X. Chen, and A. Sanchez
To be published in IEEE Trans. Magn.

18. 'Demagnetizing Factors for Completely Shielded Rectangular Prisms'
E. Pardo,D.-X. Chen, and A. Sanchez
To be published in J. Appl. Phys.

19. 'Equilibrium positions due to different cooling processes in superconducting systems'
C. Navau, A. Sanchez, E. Pardo, and D.-X. Chen
To be published in Supercond. Sci. Technol.

20. 'Magnetic granularity analysis of YBCO coated conductors'
A. Palau, T. Puig, X. Obradors, A. Usoskin, H. Freyhardt, L. Fernandez, B. Holzapfel, R. Feenestra, A. Sanchez, and E. Pardo
To be published in Physica C.

21. 'Theoretical analysis of ac susceptibility and ac losses in superconducting tapes containing horizontally aligned filaments'
E. Pardo, D.-X. Chen, A. Sanchez, and C. Navau
To be published in Inst. Phys. Conf. Ser.